Quantifying lahar damage using numerical modelling: response and list of changes

Stuart R. Mead, Christina Magill, Vincent Lemiale, Jean-Claude Thouret and Mahesh Prakash

Again, we would like to thank the reviewers and editors for their time taken in review of this manuscript. A broad response to reviewers' comments has already been provided (see http://www.nat-hazards-earth-syst-sci-discuss.net/nhess-2016-282/#discussion). This list of changes forms a point-by-point response to each reviewer with changes noted.

Each change is noted and tracked in the document that follows these responses. For convenience, we have summarised the major changes as the following:

- Moved detail on the calculation of bending moments and ultimate strength to appendices.
- Added detail (in appendices) on calculation of shear strength.
- Merged Lahar rheology section with Implementation in smoothed particle hydrodynamics section.
- Added subsections to discussion highlighting, critically evaluating and justifying assumptions.
- Improved figures 1-6 and 9-13 in response to reviewers comments.

Sincerely,

Stuart Mead

Point-by-point response

Reviewer	Summary of reviewer's Comments or Requirements	Corrections/amendments made	Revised page/line reference
General/title and abstract comments			
Reviewer 1	Building vulnerability: A general confusion is created by the use of building types from other studies (Thouret et Al., 2013, 2014) which are referred to as building vulnerabilities. Clearly define what you mean by vulnerability.	We are now referring to these as simplified structural classes. An additional table that provides a description of each building type and typology and their simplified structural class has been included.	NA
Reviewer 1	Building vs block: it is not always clear throughout the paper what you are taking into account for your modeling and how data is aggregated. … There is more explanation needed here.	Building, block and block orientation will be comprehensively discussed in the Case study section, highlighting the relationship between them. Figure 2 (which will be modified) and Table 1 also help to explain the number of buildings per block, and composition.	NA
Reviewer 1	Lahar rheology and modeling: A lot of detailed description is provided on lahar rheology with the result that the reader remains relatively confused facing a complex topic with lots of	We have reduced the amount of discussion on lahar rheology to focus only on the core details needed to understand this study. Additional explanation on SPH and why it was chosen over other approaches (also explained) is provided.	NA

	technical terms in a few paragraphs. It is not clear from the structure of the text, what objective this section serves. A reorganization of this section might help to outline more specifically why the SPH model has been chosen, what its differences are compared to more commonly used lahar modeling software and what interest the use of this model has in terms of creating the depth-pressure curves.		
Reviewer 1	Structural failure model similar to those employed by Roos (2003): Roos (2003) made his classifications and his study (comparison of the loads on the structure with the strength of the structures) for masonry buildings in the Netherlands, so the transposition for Arequipa buildings should be argued.	This is addressed in an expanded 'limitations and discussion' section and explanation of bending moment calculations.	NA
Reviewer 2	Lines 315-323: Please check if the concepts of "normal stress" is more appropriate than "normal pressure component". Line 305: The "directional components of the dynamic pressure ...". Pressure, and dynamic pressure are scalars (see above)	We have modified text to ensure our consistency with established terminology through the manuscript.	NA

Reviewer 1	Title Better: lahar induced damage	Title changed to 'Examining the impact of lahar on buildings using numerical modelling'	NA
Reviewer 1	Line 15: What is the "relative importance" of lahar hazard, etc.?	'Relative' as a word is irrelevant here, changed to "…examine the importance of lahar hazard..."	16
Introduction			
Reviewer 1	Line 24/25: may add here Vallance (2000) as a reference	The reference to Vallance and Iverson (2015) is from the second edition of Encyclopaedia of Volcanoes were Vallance (2000) is from the first. They are functionally the same work.	25
Reviewer 1	Line 28: again, careful with the word "uncertainty" here, I think it is not adequate	Changed to '…varying number of elements…" here and in the abstract.	28
Reviewer 1	Line 34: clarify "relative" – is this from a statistical point of view?	See previous response, 'relative' is removed.	34
Reviewer 1	Line 75: "to identify strategies that may reduce building loss" – these strategies appear to be mentioned only in a short paragraph in the conclusion which appears quite disconnected from the rest. If this really is one of your objectives, this needs more argumentation and	Rather than strategies to reduce loss, the aim is better described as investigating the role of hazard (flow rate and rheology), exposure (building orientation) and vulnerability (building quality/type) components on building loss in Arequipa. This has been corrected and is consistent throughout the manuscript.	76ff

	be put in relation in a more concrete way with your modeling results.		
Case study: Quebrada Dahlia, Arequipa, Peru			
Reviewer 1	Line 86: watch the spelling – torrenteRAS, one R at the end	Fixed throughout manuscript.	88
Reviewer 1	Line 93: cite also and in first place Martelli 2011	Added per NHESS reference style (chronological).	90
Reviewer 1	Line 109: "relative effects" – again, don't understand the use of the word relative here. Be more precise.	Again, 'relative' is irrelevant in this context.	111
Reviewer 1	Line 118: I don't understand the use of "by" here before cross streets. Does this mean the cross streets and quebrada separate the buildings in a way that blocks are formed?	Modified figure 2a and reworded sentence to clearly explain how the buildings are separated into to five city blocks.	121
Reviewer 1	Line 119: the "general approach" needs to be explained at least in a few sentences for those who do not have the time to read Thouret et al (2014).	The following sentences explained the building classification method of Thouret et al. (2014), this has been reworded to make it clear.	123

Developing building vulnerability relationships			
Reviewer 1	Line 133 and 135: Need to give more detail on these models/approaches.	A brief description of the concept of these approaches has been provided.	139-141
Reviewer 1	Line 134-135: this is a very important assumption “Stresses for buildings in Arequipa are calculated using the approach specified in Australian Standard (AS) 3700-2011” and some better explanations should be provided. Line 135-136: Reformulate the sentence; it is not clear what you mean here. Line 137: “While some specifications in the standard may not be relevant for Arequipa, the calculation method is still valid for the area provided construction material properties from Arequipa are used as inputs.” Yes, some specifications in the standard are not relevant for Arequipa, and the calculation method are not just related to the material properties, but also to the construction mode and the behavior, so “the methods are still valid” is not necessarily obvious, but should be argue in this way.	These comments have been dealt with simultaneously. A better explanation of why the standard can be relevant for Arequipa is provided, and the effects of this assumption is mentioned here and discussed in the reworked discussion section.	129-158

Reviewer 1	Also important simplification or assumption "In these models, masonry walls are presumed to fail when the applied bending moment and shear forces are greater than the calculated ultimate bending moment and shear force the walls can withstand. We only consider the maximum bending moment here as preliminary investigations suggested the force required to overcome the ultimate moment was consistently lower than the force required overcoming the ultimate shear force". This should be justified by literature investigation, experimental test or numerical simulation. The behavior of masonry wall is quite complex and can be (or generally is) a mix of flexural and shear behavior, in this case, considering just the maximum bending moment is an important assumption that can affect the global results and conclusions. See macroelement masonnery behaviour software TREMURI paper S. Lagomarsino, A. Penna, A. Galasco, S. Cattari, TREMURI program: an equivalent frame	The response to shear is important to consider, however the effect of this is minimal in our study. In an effort to simplify the manuscript we chose to leave discussion of shear out of the manuscript. However, for the reasons you identified, this was probably not the best idea. Instead, we have added additional information on the shear response in an appendix and made reference to it in this section. This way, the focus of the manuscript is maintained, but additional information is available to readers if needed.	147

	model for the nonlinear seismic analysis of masonry buildings, Eng Struct, 56 (2013), pp. 1787–1799. Line 139: “preliminary investigations” – of what? Lab tests? Modeling? Field work?		
Reviewer 1	Moreover, when we use “design capacity specified in actual standards” for the constructions that have certainly “no design” or, in the better case “low code design”, this affect the results and cannot be considered as representative for the studied area.	This has been partly addressed and discussed further in the limitations and discussion section.	151ff and 350ff
Reviewer 2	In equation (1), b is referred as the thickness of the bricks used in the wall (see line 145). Later, at line 147, b is referred as the wall thickness. This is different for walls with a thickness greater that the width of a single brick. Do you consider only walls made of a single layer of bricks?	Here, we assume that brick and wall thickness are equal (i.e. only single layer walls), as observed in the field investigation – this has been clarified in the manuscript and *b* now consistently refers to wall thickness when appropriate.	145
Reviewer 1	Line 146: “should not be greater than this value” – Why? Explain for those not familiar with this context.	Details on the calculation of bending moment has been moved to the Appendix. We have placed a short explanation in the Appendix that 0.2 MPa is the maximum tensile strength that can be assumed without	448

		testing. This assumption is critical, and is explained and discussed in the limitations section.	
Reviewer 2	Line 149: In this context, I suggest to specify that the "normal forces" are vertical forces.	Thank you for the suggestion, this has been changed in the appendix and helps in reducing confusion between terms.	451
Reviewer 1	Line 150 and following: quite a lot of equations and parameters presented. Since you are basically using parameter values specified in the Australian Standard, it may not be absolutely necessary to detail all of these equations. Line 169 and following: a little graphic illustration would be SO helpful here!	Details on calculation of ultimate moment (and now shear) have been added to the appendix as these components have been described previously (e.g. Zheng et al. (2009)) and are in standards.	440ff
Reviewer 2	Line 170: Symbol a→ a_v	Changed	471
Critical depth-pressure curves			
Reviewer 1	Line 186 and following: I am not able to follow here, there are too many classes from different sources, I got lost. Can you present this in an easier way than A0, 1A-2B etc.? Or at least provide an informative table describing what these mean?	A new table (Table 2) has been constructed relating building type, general description and structural class to help understanding of this and the previous sections.	689

Reviewer 2	Line 190: “The critical height”. Do you mean “The critical depth”?	Correct. Height vs. depth inconsistencies have been fixed throughout the manuscript, depth is used throughout.	169
Reviewer 1	General remark: you are analyzing vulnerability of buildings so it is a little strange to use already defined vulnerability classes. It would sound more logical to refer to simple building types or categories for the Thouret et al classifications instead of calling these vulnerability classes.	We agree that ‘vulnerability class’ is a confusing term, we now refer to the classes as structural or simplified structural classes throughout the manuscript.	NZ
Reviewer 1	For figure 4, you mean that the graphic represents the combination between the depth and the dynamic pressures for which you have failure of the building class? This could be assimilated as a limiting right under the line you do not have collapse and above the line you have collapse? In order to verify the results for one structure or one wall it will be interesting to perform a kind of push-over curve (curve displacement-shear base response).	We have slightly rephrased the text surrounding figure 4, discussing, as the reviewer states, that the curves indicate the structural limit of each class. Depth-pressure combinations above the line exerts forces greater than the building can withstand, however the damage (e.g. collapse vs. partial collapse vs. weakening/cracks) caused by these forces is still likely to be proportional to the magnitude of the excess forces. While we would like to extend this work into determining proportional losses, the (current) lack of data and observations limits us in this regard, this is discussed in the limitations and discussions section.	170ff
Reviewer 1	Maybe a table with the description of the building types from 1A to 6C would be useful	Table 2 (new) provides a description of each building type and structural class. To help with self-understanding, a shortened	Fig. 4

	for self-understanding of the paper accompanied by the building damage threshold for each typology (these thresholds are a very important issue, that can modify completely the results, and in my opinion this issue is not sufficiently treated in the paper).	description for each class is added to figure 4. The extended discussion goes into further detail on the use and assumptions of damage thresholds.	
Reviewer 1	Line 195 and following: OK, but is this representative? Most hyperconcentrated flows in Arequipa carry boulders given the environment there, and the impact of those is very important although not taken into account at all in your study …	The simple answer here is yes, boulder induced damage is critical for determining lahar induced damage. This is already noted throughout the manuscript (lines 56 – 65, 127 – 128, 383 – 390). However, boulder damage (at least, a flows' boulder carrying capacity) is proportional to depth and dynamic pressure (*velocity*). In this study, we see that a large amount of damage will occur even without boulders, and that exposure (the proximity and orientation of houses relative to the quebrada) dominates. In this context, detailed studies of boulder carrying, sizes etc. are less important compared to quantifying (and trying to reduce) the exposure. The effect of boulders on lahar damage is addressed in the discussion of assumptions.	
Lahar rheology (*now 'Lahar rheology and implementation in smoothed particle hydrodynamics'*)			
Reviewer 1	General remark: This is a long overview but it is not clear why you expose all this to introduce finally the quadratic rheology model. Rewrite	This section has been greatly simplified and combined with the following section. Critical terms (non-Newtonian, Newtonian, etc.)	184-222

	this section illustrating from the beginning the quadratic rheology model and how it compares to other existent models and explain your choice rather than the general information which is rather disconnected from the rest. Also, you are using a lot of technical vocabulary here concerning the rheology which some part of the readers may not be familiar with. So, simplify and rather concentrate on providing definitions of critical terms such as non-Newtonian, Newtonian, etc.	are defined, and an explanation of how this compares to other models has been provided.	
Reviewer 2	Line 223: Usually the coefficient μ (eq.7) is defined "viscosity" only when the exponent m is equal to 1.	This equation has been removed from the revised manuscript.	NA
Reviewer 1	Line 246: OK, but you need to describe at least a little bit what this model is and how it is different from classically used lahar modeling software such as Titan2D/3D, LaharZ, etc.	A summary of the common modelling approaches (such as Titan and LaharZ) and why they are unsuitable for this study is provided, along with an explanation of why SPH is used in this application.	196-200
Reviewer 2	Line 252: "equation 3". Perhaps you mean eq. (7) or (8)?	References to equations are corrected.	209ff

	Lines 256 and 262: "equation 4"? Perhaps eq.(7)? Please check		
Reviewer 1	Line 257f: Again, I got lost here – what is your point?	The purpose of viscosity regularisation is to reduce computational cost; this is highlighted better in the revised manuscript. These technical details are crucial for readers who may want to reproduce the approach, but is kept as brief as possible for readers not familiar with modelling/terminology.	214
Reviewer 1	Line 263: Where is m in the equation? How many validation simulations did you use and what data was chosen for it?	This is a typo, we have changed to parameter "*c*" and added more explanation on why it was set to 200 (validation against analytical results).	219
Lahar simulations			
Reviewer 1	Line 268: "may not represent any specific event…" So what is the use of it? This is not at its place here. You may have a general discussion section where such issues should be discussed, but at this point, the reader may not think it is useful to continue the reading.	We have provided a better explanation of the choice of scenarios, and have highlighted the effect of these choices in the discussion section as appropriate. A clearer aim for the manuscript ("…investigate the effect of hazard (flow rate and rheology), exposure (building orientation) and vulnerability (building quality/type) components on building loss in Arequipa") also helps to address this comment.	224-235

Reviewer 1	Line 269: 12.5 cm resolution? At this resolution, the identified building blocks and houses should be much more accurate than what appears in Figure 2 and Figure 5!	The final terrain model resolution is lower than this (this detail was missing in the initial manuscript and has been added to the 'Case study' section). SPH particle resolution is usually finer than terrain resolution, as in this case, to resolve important features of the flow. The resolution was chosen from a similar (preliminary) study in Mead et al. (2015) – referenced.	119
Reviewer 1	Line 281: Again, remind what these stand for and why you can take the experimental values for Arequipa.	All symbols have now been clearly explained.	238ff
Reviewer 1	Line 286: Hyperconcentrated flows can have high viscosities, no?	Correct, the viscosity of our hyperconcentrated flows were ~10 times higher than that of clear water (see table 3). We understand the confusion of this sentence and have reworded it to highlight that dispersive stresses are higher in our debris flows.	246-248
Reviewer 1	Line 289: 45 seconds: why? Computational time and resulting cost? Maybe optimize this paragraph.	This paragraph (line 289 to 291) is rewritten to address these comments - computational time (cost) limited the simulations to 45 seconds and therefore our scenarios most represent the damage	249-252

	Line 290f: I do not agree here. Lahar surges do not always have higher depths than a steady lahar flow. First, a steady lahar flow is not necessarily the opposite of a lahar surge but a different flow type/phase. Second, the surge can be quite small and there can be several small surges before the major lahar flow front arrives. It depends a lot on the location and the environmental conditions triggering the lahar. So careful here to not make it sound as a general rule.	caused by higher velocity and depth surges/waves in lahars than steady lahar flow.	
Flow behaviour			
Reviewer 1	Line 297ff: Not clear. What is your point here? Line 300: This is not new…	Lines 294 – 302 are a brief description of the main flow features shown in Fig. 5 to help the reader in their interpretation and highlight aspects that are important for the following discussions – so is not necessarily highlighting things that are 'new', but making observations clear. This paragraph has been reworded (including removing the unclear sentence on L297).	254-262
Reviewer 1	Line 300ff: Decreasing velocity can also be due to friction effects and turbulence along the channel walls.	Different friction effects and turbulence are a result of the differences in rheology, this point has been added.	259

Reviewer 1	Line 308: "buildings oriented parallel to the channel": this depends how you define the long axis of the building. Looking at Figure 2, this is not very clear to me. What do you mean by "broad understanding of normal pressure"?	Our explanations of buildings, blocks and orientation to the channel are improved in the case study section. We have changed the sentences surrounding L308 to make it clear we are talking about orientation of walls (not buildings). Bad grammar of "broad understanding of normal pressure" fixed ("…initial").	265-278
Reviewer 1	Line 313: illustrate this with a graphic illustration. "Higher EW pressures …" Not sure I understand what you mean. Flow looses velocity and depth when spreading in side-roads?	The descriptions around pressure actions have been modified. We believe this may help the reader understand the reasoning better than a figure might.	270-275
Reviewer 1	Line 316: Pressure magnitude: you need to define this term. Line 323: normal pressure: need to define this term!	In response to reviewer #2's comments, this has been refined by modifying the flow behaviour section to add discussion on the calculation of dynamic pressure is calculated and explain the difference between using the velocity magnitude (scalar, not normal to walls) and normal velocity to determine forces exerted on the walls.	279-285

Reviewer 1	Line 329: you were mentioning earlier that you consider only initial lahar surges, so this is not really a conclusion of the modeling, is it?	Correct, this has been removed.	296
Reviewer 1	Line 330: Why is this a consequence of the short timeframe?	We have expanded an earlier (critical depth-pressure curves) part to explain that equalisation of hydrostatic pressure requires the fluid to enter the building and rise to the same height as the outside. This takes a reasonable amount of time, much less than the duration of the surges modelled here.	296-298
Reviewer 1	Line 334: "higher pressures": you mean higher dynamic pressure?	Correct – changed.	301
Reviewer 1	Line 335: If this indicates elevation differences, it would be helpful to have a map illustrating what elevation differences there are in this study area.	This wording has been refined, it refers to elevation of the cross-streets.	302ff
Reviewer 1	Line 336: acting on blocks: rather buildings?	This paragraph has been reformulated to refer to walls. Data from the simulation is obtained per-block (which is now explained in an earlier paragraph), so we take care to describe the affects related to the block, rather than individual buildings.	304-309
Reviewer 1	Line 337ff: reformulate, this paragraph is not clear. Also, I am skeptical that higher density generally causes larger dynamic pressure …can you provide reference?	As pressure is proportional density time the square of velocity, for the same velocity, dynamic pressure will be larger. See Jenkins et al. (2015) as an example. We have reformulated the paragraph to describe the differences in dynamic pressures between rheologies.	306

Reviewer 1	Line 338: near perpendicular walls: and not near, what happens?	The difference between pressures applied to perpendicular and parallel walls has now been explained in this paragraph.	304-309
Reviewer 1	Line 340: The dilatant component is lower for debris flows than for Newtonian and hyperconcentrated flows, so the latter decrease in velocity quite rapidly when diminishing in depth which also reduces the pressure for these flows…	The dilatant component is much higher for debris flows than hyperconcentrated and Newtonian flows – see table 2. The reformulated paragraph relating pressure differences to rheology should help to limit confusion on the effects of rheology on dynamic pressures.	304-309
Application of critical depth-pressure curves			
Reviewer 1	Line 342: "along the block" – means what?	Changed to "…pressure acting on block walls…". Building, block and orientation descriptions are defined earlier in the manuscript. Explanation of how pressures are obtained also clarifies this meaning.	311
Reviewer 1	Line 348f: Not clear, "well above the critical curves for each block". General remark: you switch between buildings and blocks and it is in the end not very clear for what you realize your modeling and how do you generate the curves	The role of the critical curves, difference between buildings and blocks are all explained in earlier sections to make this part clearer.	Previous.

	for one block? Is it the mean value of all buildings contained in the block? In this case, we need to have more information on each block…		
Reviewer 1	Line 353: fluid height – be consistent in the use of your terms to make it easier for the reader to follow. Either use fluid height or flow depth.	Depth is now used throughout.	322
Reviewer 1	Line 354: Which means no damage to expect?	Not necessarily, this is explained in the expanded discussion section.	350ff
Reviewer 1	Line 357: lower depths? This is interesting: I would have thought that depth rises when flow impacts a perpendicular wall. At least this is what you see frequently with … it would be interesting to compare your methodology with another location and see if you find similar relationships.	Depths are lower for a number of reasons: (1) perpendicular walls are further from the channel, (2) overbank flow is occurring, meaning that the flow is not directly impacting perpendicular walls, but spreading along cross-streets and (3) velocities are generally lower in these cross-streets, reducing the size of run-up on a wall.	324-328
Reviewer 1	Line 359: “effect of vulnerability”: this means what?	This part of the sentence is more suited to discussion and has been moved.	NA

Reviewer 1	Line 371: explain in more detail what this means "reducing the size of the applied moment".	Explained in better detail; the applied moment is smaller as a result of the low depth.	340
Reviewer 1	Line 375: across scenarios: means that this can be observed in several scenarios? How many did you have in total? Other studies also indicate that distance from the channel plays a more important role than the building type itself…	Rephrased to say "…for all scenarios". Also added reference to other studies that confirm these findings (that distance is more important than building type).	344
Discussion (now *Limitations and discussion*)			
Reviewer 1	Line 380ff: Reformulate, this paragraph is not clear. Line 389: "applied to ultimate moment and damage through other actions" – how are these defined? Line 390: comprehensive data: like what?	This paragraph has been reformulated and definitions have been clearly explained.	383-393
Reviewer 1	Line 393: Repetition, see line 329	This has been moved to the previous section, as a better explanation.	Previous

Reviewer 1	Line 395ff: depends on localization of the building respective to the channel: first row, second row, screening effect, etc.	Added more detail to explain this could be an effect.	394ff
Reviewer 1	Line 409: this is not new…	This doesn't have much place in the manuscript, removed the sentence.	NA
Conclusion			
Reviewer 1	Line 416: not new	Conclusion has been changed to make this not relevant	425ff
Reviewer 1	Line 417ff: This paragraph comes somehow out of the blue and is quite disconnected from the previous rather technical descriptions. The recommendations for retrofitting are not enough put in relation with the results of your modeling, it would maybe be a better option to add this into the discussion and link it more specifically to your results.	Added these elements to the discussion.	415-424
Reviewer 1	Line 425: here you say the approach can be generalized but given all the restrictions and constraints you have for Arequipa, this sounds rather unlikely. The best way would be to propose a section where you apply this	The vulnerability calculations are necessarily specific to Arequipa, however the approach to quantifying losses (using bending moments, calculating pressures from numerical modelling) can be applied to other areas. This has been expanded in the conclusion.	425-431

	approach to a different study area and shortly explain how you validate your approach. Or you need to explain more in detail why and how this approach can be generalized.		
Reviewer 1	Line 429: Large-scale indicators: such as? Line 430: In my opinion, you are not modeling vulnerability. You use building type data, do lahar modeling and cross this information to generate building performance curves… Line 431: "refine the indices in order to focus": only if data is available as for now you use a lot of data extrapolated from other sources.	The conclusion will be largely rewritten to reinforce the main 'novel' aspects of this work. These are valid comments, and have been taken into consideration when writing the conclusion.	425-438
Figures and tables			
Reviewer 1	Figure 1: need to complete the legend indicating what the yellow and orange lines stand for as well as the orange areas (built area: extent of the city at present?); reduce the size of the North arrow. The NE end of the quebradas Venezuela, Huarangal and Andamayo are quite low and appear disconnected from the foothill of the volcano – is	We have modified this figure and the caption to improve understanding. This is a simplified map to set the context for readers.	

	there a reason for this presentation?		
Reviewer 1	Figure 2: I think you need to better define what you understand by building block. Since you refer a lot to the works of Thouret et al. 2013 and 2014, his definition of building blocks seems to be different from what you delineate here as a block. Clarify. Also, the delineation of your blocks is not easy to understand: for example in fig. 2B, bottom left, you distinguish three blocks dark green, light green and dark blue; on the opposite side of the road, the light violet block appears to be a single block although you might also have distinguished at least two; same for the light green block further North on the right side … if so is your choice, at least explain how you determine.	Additional explanation has been added to the Case study section of the manuscript to improve understanding of buildings and blocks.	
Reviewer 1	Figure 3: title of legend "Design compressive stress" – means what? Is it the compressive stress? "Building Type" – no capital letter for type.	Added explanation of "Design compressive stress" to the caption (the compressive stress the building can withstand according to the standard). Modified Building type axis label.	

Reviewer 1	Figure 4: Maybe simplify where possible this group of graphics: no need to put the “depth” legend title everywhere; reduce the appearing scale numbers (no need to detail every 0.25, just indicate 0,5; 1 and leave the little markers for subunits). There is a lot of information presented, so simplify a maximum.	Simplified figure following these recommendations.	
Reviewer 1	Figure 5: what do the arrows indicate on the lower left of each image? Images are quite small text is a little too big. Might be helpful to have an image without any modeling result where you locate the channel limits, outline the buildings and indicate flow direction. Figure 6: same remark as above; legend too big, no need to reproduce the same legend for all three image groups. The pressure value to the left is too isolated, difficult to understand what this means.	Made images larger, reduced size of the text and modified arrows (indicates North). The channel limits and buildings are outlined in Figure 2 (now modified slightly to explain this).	
Reviewer 1	Figure 9, 10 and 11: Difficult to distinguish the individual curves: maybe fine lines of different colors would be easier to read here.	Made lines finer to help distinguish curves.	

Reviewer 1	Figure 12 and 13: Legend title “loss fraction” is a little strange not associated with percentages. Flow rate needs a unit! For the rest: same remark as above: simplify.	Simplified plots, modified loss fraction to percentages.	
Reviewer 1	Table 1: Associate table with a figure where these numbers can be seen.	Association to figure 2c included in caption.	
Reviewer 1	Table 2: OK – I am not an expert in streamflow/lahar rheology, so I am not able to evaluate the correctness of these parameters. However, I understand these parameters are not your own modeling results but used to model, so provide reference for the source of these values in this table.	References added to the table.	

Examining the impact of lahars on buildings~~Quantifying lahar damage~~ using numerical modelling

Stuart R. Mead[1,2], Christina Magill[1], Vincent Lemiale[2], Jean-Claude Thouret[3] and Mahesh Prakash[2]

[1]Risk Frontiers, Department of Environmental Science, Macquarie University, Sydney, Australia
[2]Commonwealth Scientific and Industrial Research Organisation, Clayton 3168, Victoria, Australia
[3]Université Clermont Auvergne, CNRS, IRD, OPGC, Laboratoire Magmas et Volcans, F-63000 Clermont-Ferrand, France
~~Laboratoire Magmas et Volcans UMR6524 CNRS, IRD and OPGC, University Blaise Pascal, Campus Les Cézeaux, 63178 Aubière , France~~

Correspondence to: Stuart R. Mead (Stuart.Mead@mq.edu.au)

Abstract. Lahars are volcanic flows containing a mixture of fluid and sediment which~~that~~ have ~~caused~~ the potential to cause significant damage to buildings, critical infrastructure and human life. The extent of this damage is controlled by properties of the lahar, location of elements at risk and susceptibility of these elements to the lahar. Here we focus on understanding lahar-induced building damage. Quantification of building damage can be difficult due to the complexity of lahar behaviour (*hazard*), ~~uncertainty in~~varying number and type of buildings exposed to the lahar (*exposure*) and the uncertain susceptibility of buildings to lahar impacts~~nduced damage~~ (*vulnerability*). In this paper, we quantify and examine the ~~relative~~ importance of lahar hazard, exposure and vulnerability in determining building damage with reference to a case study in the city of Arequipa, Peru. Numerical modelling is used to investigate lahar properties that are important in determining the inundation area and forces applied to buildings. Building vulnerability is quantified through the development of critical depth–pressure curves based on the ultimate bending moment of masonry structures. In the case study area, results suggest that building strength plays a minor role in determining overall building losses in comparison to the effects of building exposure and ~~lahar hazard properties such as~~ hydraulic characteristics of the laharflow~~.~~

Keywords lahar · hazard · building vulnerability · rheology · simulation

Formatted: Not Highlight

Introduction

Lahars, defined as gravity-driven flows containing a mixture of volcanic sediment and water (Vallance and Iverson, 2015), have caused severe damage to infrastructure and buildings (e.g. de Bélizal et al., 2013; Pierson et al., 2013; Ettinger et al., 2015; Jenkins et al., 2015) in addition to being responsible for a large proportion of volcanic fatalities (Auker et al., 2013). Assessing the extent of potential lahar damage can be difficult due to the complexity of flow behaviour, varying ~~uncertainty in the~~ number of elements (e.g. buildings and bridges) exposed to lahars ~~(e.g. buildings and bridges)~~ and a lack of knowledge in the structural capacity of these elements to withstand damage causing components of the lahar flow. Using the common definitions of Varnes (1984), we define the damaging components of lahar flow (e.g. velocity, depth and ~~density~~pressure) as the hazard; environmental characteristics of exposed elements (e.g. building locations and orientations) as the exposure; and the ability of exposed elements to withstand the hazard (e.g. building strength) as vulnerability. Lahar induced damage is controlled by the interactions ~~between~~ of these factors; however, the ~~relative~~ importance of each

component can vary. Here we focus on quantifying and examining the ~~relative~~ role of ~~importance of~~ hazard, exposure and vulnerability in determining lahar induced building damage.

Post-event field assessments of building damage can elicit information relating lahar hazard to structural damage. However, these ~~field~~ assessments tend to only record information on substantial damage, are affected by terrain changes during the event which alter~~s~~ exposure, and often rely on a-priori assumptions of building strength and vulnerability (Ettinger et al., 2015). Pre-event assessments are affected by the lack of reliable hazard intensity measures (van Westen et al., 2006; Ettinger et al., 2015), differences in spatial and temporal scales, uncertainty surrounding site-specific lahar triggers (Di Baldassarre and Montanari, 2009), and a lack of structural information on building stock (Ettinger et al., 2015). These issues are reflected in the relative lack of studies on hazard impact in urban areas (Jenkins et al., 2015) and often results in a reliance on expert judgement to develop vulnerability models for lahars and flash floods (Ettinger et al., 2015).

The physical vulnerability of buildings, defined as the susceptibly of a building to damage with respect to the hazard (Künzler et al., 2012), is a function of building characteristics such as size, shape, age, construction materials, structural integrity, maintenance and build quality (Martelli, 2011; Künzler et al., 2012; Ettinger et al., 2015). Information on these building properties is often lacking and hard to collect on a large scale. This commonly~~often~~ leads to the simplification of vulnerability into a measure that can provide a relative indication of vulnerability and consequent damage (Künzler et al., 2012). Studies simplifying vulnerability into a relative index use a combination of qualitative and quantitative metrics obtained through building surveys, interpretation of remote sensing data and GIS techniques to map and analyse vulnerability on a large scale (e.g. Lavigne, 1999; Künzler et al., 2012; Galderisi et al., 2013; Thouret et al., 2013; Thouret et al., 2014; Ettinger et al., 2015). These methods can be applied to understand and highlight spatial patterns in vulnerability; however, as a relative measure, they cannot provide guidance on absolute ~~expected~~ damage for any specific event.

A direct estimation of damage caused by specific events requires quantified relationships describing a buildings response to the hazard. Buildings can be damaged through a number of mechanisms including: (i) direct damage resulting from static and dynamic forces imposed by the flow; (ii) damage to foundations through erosion and scour; (iii) buoyancy effects of the flow causing structures to float; (iv) direct damage from larger debris (missiles) within the flow; and (v) indirect damage caused by chemical and biological actions such as seeping induced weakness of mortar (Kelman and Spence, 2004). All these actions, ~~with the exception of~~apart from chemical and biological effects, are related directly to lahar depth, velocity or a combination of depth and velocity. ~~As a result~~Thus, a common approach in determining building damage thresholds for a particular building type is to relate damage to hazard intensity measures of depth and/or velocity (e.g. Zanchetta et al., 2004; Custer and Nishijima, 2015; Jenkins et al., 2015). However, building typologies are affected by socio-economic, cultural and institutional conditions (Künzler et al., 2012) and hazard intensities (flow depth and velocity) are affected by building environmental ~~and environmental~~ factors such as local elevation, distance from main channels and orientation ~~affect flow depths and velocities near buildings~~ (Thouret et al., 2014)~~.~~. This results ~~resulting~~ in complex interactions between hazard, exposure and vulnerability. These issues cause direct vulnerability relationships to be site-specific and requires detailed investigation of the regions at risk to examine the relative effects and roles~~importance~~ of hazard, exposure and vulnerability on building loss.

We attempt to quantify and examine the components that determine building damage in a small area within the city of Arequipa, Peru. A relative index of vulnerability on a city-block scale was developed for Arequipa in

Thouret et al. (2013) and Thouret et al. (2014). The studies by Thouret et al. highlighted two groups of vulnerability indicators~~,~~ ~~–~~(building characteristics and the physical setting~~,~~) that play an important role in determining vulnerability within Arequipa. In this study, we separate the building characteristics (i.e. vulnerability) from physical setting (i.e. exposure) ~~in order to~~to examine the effect of hazard (flow rate and rheology), exposure (building orientation and location) and vulnerability (building type) ~~identify components most~~ components on ~~strategies that may reduce~~ building loss within Arequipa. Physical vulnerability of buildings is explicitly separated from exposure through the development of a building damage model dependent on flow velocity, depth and sediment concentration. Simulations of lahar flow using smoothed particle hydrodynamics are used to examine how flow characteristics and the physical setting of city blocks affects forces on buildings and the consequent damage. While, for reasons explained earlier, damage functions presented here are necessarily specific to Arequipa, the hazard modelling approach and vulnerability model development are described in detail to support risk assessment in other regions affected by lahars.

Case study: Quebrada Dahlia, Arequipa, Peru

The central business district of Arequipa, the second largest city in Peru, is situated 17 km southwest of the summit of El Misti (Fig. 1), a steep stratovolcano with a history of explosive eruptions. Rapid population growth since 1960 has resulted in an expansion of the city towards the ring plain and steep slopes of El Misti (Thouret et al., 2013). Arequipa is drained by several ravines (locally called quebradas or torrenter~~r~~as), shown in Fig. 1, that have been shaped by lahars and floods originating from the volcano on volcanoclastic fans northeast of the city. These quebradas are normally dry but carry water sporadically during the December to March rainy season (Vargas Franco et al., 2010; Martelli, 2011; Thouret et al., 2013; Sandri et al., 2014). Flash floods and hyper-concentrated flows occur relatively frequently in the quebradas, with return periods between 2 and 10 years (Vargas Franco et al., 2010; Thouret et al., 2013). Previous studies of lahar hazard and vulnerability for Arequipa identified seven alluvial terraces (T0, T1, T1', T2, T2', T3 and T4) based on stratigraphy and local elevation above the quebrada and the Rio Chili valley (Martelli, 2011; Thouret et al., 2013; Thouret et al., 2014). The likelihood of inundation by a lahar or flash flood decreases with each terrace. Terrace levels T0 and T1 (up to 3m above the quebrada) are frequently flooded (approx~~i.e~~. every 2 to ~~-~~10 years). The higher terraces (T1' to T2', 3 to 10 m above the quebrada) are rarely flooded (estimated 20~~-~~ to 100 years) and the highest terraces (T3 and T4) are only likely to be inundated by lahars linked to large eruptions (Thouret et al., 2013; Thouret et al., 2014). A city wide vulnerability study by Thouret et al. (2014) identified that the city blocks most vulnerable to flash floods and lahars were on lower terraces and typically within 100 metres of a quebrada.

To build on this study and investigate the vulnerability of the quebrada channel and banks in detail, simultaneous photogrammetry and building surveys were undertaken along short sections (approximately 200 m) of several quebradas during September 2013. Here we focus on one 150 m long section of Quebrada Dahlia to examine lahar hazard and building damage. Quebrada Dahlia is a small tributary of Quebrada Mariano Melgar-Huarangal (Fig. 1), which is situated in the Mariano Melgar District on the north-easternmost fan of Arequipa, shown in detail in Fig. 2. The case study area was chosen for the following reasons:

- The quebrada channel is ~~relatively~~ reasonably straight, reducing the effect of bends in the watercourse on lahar dynamics.

- Building quality varies from well-built reinforced masonry buildings to makeshift structures with little to no mortar. This allows for an investigation of the ~~relative~~ effects of building quality on damage caused by lahars.
- All buildings are situated on the lowest terraces (T0 – T1', 1 - 5 m above the channel), meaning they may be affected by even the smallest events identified in Vargas Franco et al. (2010) and Thouret et al. (2013).

A three-dimensional reconstruction of the terrain and buildings along Quebrada Dahlia was created using the photogrammetry method described in Mead et al. (2015). The ~~generated~~ surface reconstruction~~terrain model~~, shown in Fig. 2b, contained 1.4 million points with a surface density of between 150 and 750 points per m^2. A~~, a~~ GNSS-D survey undertaken in October 2014 enabled geo-referencing of the terrain reconstruction for possible inclusion in future GIS applications. The surface reconstruction was smoothed and reduced to create ~~the~~ a lower-resolution terrain model shown in Fig. 2c~~,~~ to be ~~hat was~~ used in the lahar simulations. The terrain model in Fig. 2c contains 22 buildings identified~~The reconstruction, shown in Fig. 2c, contains 23 surveyed buildings~~ during building surveys in 2013. ~~.~~ ~~Streets and the quebrada (shown in Fig. 2a) separate T~~these buildings ~~are separated~~ into five city blocks (labelled in ~~see~~ Fig. 2c~~a~~), ~~five groups,~~ referred to hereafter as 'blocks'~~., by cross streets and the quebrada.~~ ~~Typology of each building was characterised through surveys undertaken in 2013 following the approach of Building surveys were undertaken in 2013 and used the general approach of~~ Thouret et al. (2014). In this approach, buildings are classified as one of ~~Buildings were separated into~~ 8 structural types (1A – 8C) ~~depending~~ based on a visual inspection to determine ~~on~~ construction material, roof type and structural support (see Table 1). These types were then grouped into larger ~~groups of~~ simplified structural ~~vulnerability~~ classes. Using this building classification system, the study area contains 8 class ~~type~~ *A0* buildings, 7 class~~type~~ *A* buildings and ~~8~~7 class~~type~~ *B* buildings (see Table ~~1~~2 for a description of building types and structural classes)~~)~~.

Developing building vulnerability relationships

Buildings and infrastructure can be damaged through a variety of mechanisms brought upon by actions of a lahar. Here, as in most other studies of lahar damage (Zanchetta et al., 2004; Toyos et al., 2008; Ettinger et al., 2015; Jenkins et al., 2015), we focus on the direct damage resulting from hydrostatic and hydrodynamic forces applied to buildings. We regard these actions as the most important, although scour and large debris missiles within the flow can also cause significant damage (Jenkins et al., 2015). Scour and debris actions are neglected here as they are currently too difficult to predict and incorporate into large scale loss analyses (Kelman and Spence, 2004), particularly in regions with limited hazard and exposure information.

~~-~~The building stock within Arequipa is characterised mostly by masonry structures of varying quality, with some reinforced concrete structures (Thouret et al., 2014). Therefore, we develop vulnerability relationships that are primarily focused on masonry buildings. A structural failure model similar to those employed by Roos (2003), Custer and Nishijima (2015) and Zeng et al. (2015) is implemented. In these models, masonry walls are presumed to fail when the lateral pressure imposed on the wall results in a ~~applied~~ bending moment ~~and~~or shear force~~s are~~ greater than the wall's calculated ultimate bending moment or ~~and~~ ultimate shear force~~. the walls can withstand~~ ~~.~~The ultimate bending moment (M_u) is calculated using the following equation (Roos, 2003):

$$M_u = (f_t + f_d)\frac{wb^2}{6} \quad (1)$$

where f_t is the tensile strength of the masonry wall, f_d is the design compressive stress acting on the wall, w is the width of the wall facing the flow and b is the thickness of the wall, which is assumed equal to the brick width~~width of bricks used in the wall~~. Tensile strength and design compressive ~~S~~stresses for buildings in Arequipa are calculated using the approach specified in Australian Standard (AS) 3700-2011 and summarised in Appendix A in addition to ~~,~~an approach to calculating ultimate shear force. Preliminary investigations using these two approaches suggested the force required to overcome the ultimate moment was consistently lower than the force required to overcome the ultimate shear force. Therefore, we chose to focus the remainder of this study on the ultimate bending moment only.

~~While t~~The use of a foreign standard to calculate the ultimate moment ~~calculation method of a foreign standard~~ should still be valid for the study area if construction material properties from Arequipa are used as inputs. However, some specifications and assumptions of the standard may not be relevant. Notably, ~~O~~observations during the building survey suggests that construction methods and conformity to specifications within the standard differs substantially to those specified in AS3700-2011. This difference will influence ultimate bending moments, particularly those for low-quality unreinforced building types (i.e. building types 1A-2B) due to the makeshift nature of construction. For these classes, calculated bending moments will represent a 'best case' scenario where masonry unit strength and quality has not been compromised by construction methods. ~~While some specifications in the standard may not be relevant for Arequipa, the calculation method is still valid for the area provided construction material properties from Arequipa are used as inputs. In these models, masonry walls are presumed to fail when the applied bending moment and shear forces are greater than the calculated ultimate bending moment and shear force the walls can withstand. We only consider the maximum bending moment here as preliminary investigations suggested the force required to overcome the ultimate moment was consistently lower than the force required to overcome the ultimate shear force.~~

Critical depth-pressure curves

The range of design compressive stress for each building typology is shown in Fig. 3. The range was obtained by calculating the design compressive stress for every ~~realistic~~ configuration of masonry compressive strength (f_c), wall thickness ~~brick width~~ (b) and thickness coefficient (k_t) in Appendix A. Buildings with reinforced frames (types 3, 4 and 6) ~~are able to~~can withstand much greater compressive stresses than non-reinforced buildings (types 1, 2, 5). The wall thickness ~~brick width~~ has a large effect on building strength, which is consistent with observations of Jenkins et al. (2015). Notably, the design compressive stresses are similar for building types that share the same ~~vulnerability~~ simplified structural class identified in Thouret et al. (2014), based on the ~~vulnerability~~ structural classes of Zuccaro et al. (2008). Given these similarities, we also use the simplified structural ~~vulnerability~~ classes (A0, types 1A-2B; A, types 3 and 5; and B, types 4 and 6A-6C, see Table 2) from Thouret et al. (2014)~~, see~~ .

The critical ~~height~~depth (i.e. hydrostatic pressure) and dynamic pressure required to overcome the ultimate bending moment (equation 1) for each ~~vulnerability~~ structural class is shown in Fig. 4. These curves assume that both hydrostatic and dynamic pressure acts on walls. Other studies (e.g. Jenkins et al., 2015) assume only dynamic pressure acts on walls due to an equalisation of lahar depths on the inside and outside of buildings. This equalisation can take a reasonable amount of time, which is likely to be much longer than the simulation duration studied here (see following sections). The curves in Fig. 4 indicate the structural limit of each class; ~~point at~~

~~which the applied moment from hydrostatic and dynamic pressure equals the ultimate moment of the wall.~~ ~~C~~combinations of depth and pressure that fall above the curves indicate an applied moment greater than the building can withstand. Conversely, combinations of depth and pressure that fall below the curves indicate an applied moment less than the maximum the building can withstand. Figure 4 shows that the critical depth decreases with the density of ~~the~~ flows~~,~~ as the hydrostatic pressure gradient is much larger for sediment-rich lahars. The critical depths and pressures are also affected by the ~~vulnerability~~ structural class, with *A0* structures being much less resilient than *A* and *B* structures. However, wall thickness~~brick width~~ has the most dominant effect on determining the strength of buildings. Wider walls~~bricks~~ increase the section modulus ($wb^2/6$ in equation 1), resulting in stiffer walls that also have a higher compressive stress capacity.

Lahar numerical modelling and results

Lahar rheology and implementation in smoothed particle hydrodynamics

Lahar flow behaviour varies depending on the sediment concentration and composition of the flow. At very low concentrations of sediment, lahars will flow in a similar manner to water. At higher concentrations, interactions between the sediment and water cause a non-linear response to stresses applied to the flow. This non-linearity in the stress-strain relationship requires the use of rheology models that capture both the linear (i.e. water-like, called *Newtonian*) and non-linear (called *non-Newtonian*) shear response~~behaviour~~. Here we~~We~~ implement a generalised quadratic rheology model ~~using smoothed particle hydrodynamics (SPH)~~ to simulate lahar flows along the case study area. The quadratic rheology model can be expressed as (Julien and Lan, 1991; O'Brien et al., 1993; Jan and Shen, 1997):

$$\tau = \tau_y + \mu\dot{\gamma} + \alpha\dot{\gamma}^2 \quad (2)$$

Formatted: Right

where τ is the shear stress, τ_y the yield strength, μ the viscosity, $\dot{\gamma}$ the shear rate, and α is the turbulent-dispersive parameter, a coefficient that combines the effects of turbulence and dispersive stresses caused by sediment collisions. This model follows the general form of the Herschel-Bulkley equation commonly used to describe non-Newtonian lahar behaviour (Manville et al., 2013).

Commonly used lahar models such as the Pitman and Le (2005) model in Titan2D (Patra et al., 2005) or laharZ (Iverson et al., 1998) are able to delineate hazard zones or lahar inundation areas on a large scale. However, the reduced dimensions of these models (e.g. through depth-averaging in Titan2D) means they are unsuitable for the detailed modelling of lahar flow in urban environments required for this study. Instead, we implement the quadratic rheology model ~~(O'Brien et al., 1993; Jan and Shen, 1997)The bulk flow behaviour of lahar sediment-water mixtures is controlled by the relative concentration of sediment within the flow (Dumaisnil et al., 2010). In particular, the clay content and proportion of fine sediment in suspension will greatly influence the transition from a Newtonian (i.e. constant viscosity and zero shear strength) to non-Newtonian fluid (Pierson, 2005). This transition and lahar flow behaviour is affected by inter-particle interactions (collisions and electrochemical attractions), particle-bed interactions and particle-fluid interactions, the combination of which is complex and likely exists as a continuous process (Pierson, 2005). Flows can be predominantly Newtonian with sediment volume concentrations of up to 35%, provided there are few clay or fine particles present. The inter-particle interactions between larger proportions of fines or coarse sediment in the fluid will result in a small but measurable~~

~~yield strength. Flows with a non-zero yield strength are often termed hyperconcentrated (Pierson, 2005; Manville et al., 2013) and can also be characterised by a marked dampening of turbulence (Pierson and Costa, 1987). At higher sediment concentrations, particle-particle collisions and the internal friction between particles begin to dominate, causing the yield strength to increase significantly. These flows tend to exhibit commonly observed lahar behaviours such as suspension of large boulders, unsorted particle deposits and rapid consolidation of the deposit as the pore fluid drains. Viscosity of the pore fluid also plays an important role in moderating the effect of inter-particle interactions (Doyle et al., 2010). At low viscosities (e.g. water), inertial forces and particle collisions dominate energy transfer within the fluid, while at higher viscosities (e.g. with a significant proportion of clay) the energy is mostly dissipated through fluid-particle interactions.~~

~~Several single-phase rheological models have been proposed to describe non-Newtonian lahar behaviour; most of these models follow the general form of the Herschel-Bulkley equation (Manville et al., 2013):~~

~~$\tau = \tau_y + \mu\dot{\gamma}^m$ (7)~~

~~where τ is the shear stress, τ_y the yield strength, μ the viscosity, $\dot{\gamma}$ the shear rate, and m the shear power, which describes the response to shear (i.e. shear-thickening or shear-thinning). A simple rheological description for lahar flows assumes they behave as a viscoplastic material, commonly called a Bingham fluid. Bingham fluids have a non-zero shear strength and shear power, m, of 1. Flows of Bingham fluids typically have two components consisting of a basal shearing layer (shear layer) topped with a non-shearing plug layer (Rodriguez-Paz and Bonet, 2004). In more general terms, O'Brien et al. (1993) and Jan and Shen (1997) describe the total shear stress of generic sediment-water flows as being controlled by the summation of all the debris flow strength components: cohesive yield strength, Mohr-Coulomb shear stress, viscous shear stress, turbulent shear stress and the dispersive (particle collision) shear stress. At high viscosities and relatively low velocities, the turbulent stresses can be assumed as negligible (Pierson and Costa, 1987; O'Brien et al., 1993; Jan and Shen, 1997). By combining all the relevant stresses, a generalised quadratic rheology model (Julien and Lan, 1991; O'Brien et al., 1993; Jan and Shen, 1997) can be expressed as:~~

~~$\tau = \tau_y + \mu\dot{\gamma} + \alpha\dot{\gamma}^2$ (8)~~

~~where α is the turbulent-dispersive parameter, a coefficient that combines the effects of turbulence and dispersive stresses caused by sediment collisions. Rheological parameters for τ_y, μ and α were studied for debris flows by Phillips and Davies (1991) and O'Brien and Julien (1988). We chose to implement and use this quadratic rheology model for lahars as it summarises the principal components of non-Newtonian lahar behaviour, namely a yield strength, viscous effects and a dilatant (shear-thickening) effect from particle collisions.~~

~~Implementation in smoothed particle hydrodynamics (SPH)~~

~~The quadratic rheology model is implemented~~ using three-dimensional smoothed particle hydrodynamics (SPH) to simulate lahar flows along the case study area. SPH is a Lagrangian method that tracks the physical motion of interpolation points (commonly referred to as particles) through space. It is well suited to modelling free surface fluid flows, predicting and tracking the motion of dynamic objects within the flow (e.g. Cleary et al., 2012; Prakash et al., 2014; Cleary et al., 2015), and modelling complex flooding scenarios involving interactions with buildings (e.g. Mead et al., 2015). The SPH method used here is described in Cleary and Prakash (2004) and Prakash et al. (2014). Non-Newtonian lahar rheology was implemented in SPH using an apparent Newtonian viscosity (η). Assuming the fluid is isotropic, constitutive equations for rheology can be written as a generalised Newtonian fluid in terms of the apparent viscosity:

Formatted: Justified

Formatted: Justified

Formatted: Normal

$$\tau = \eta\dot{\gamma} \quad (93)$$

When the apparent viscosity is constant the fluid is Newtonian with a viscosity of η. Non-Newtonian fluids can be modelled using equation 3 by developing relationships for η based on constitutive equations (Mitsoulis, 2007). Using this approach, the apparent viscosity for the quadratic rheology is:

$$\eta = \frac{\tau_y}{\dot{\gamma}} + \mu + \alpha\dot{\gamma} \quad (410)$$

Here, To reduce the computational time we also use the viscosity regularisation approach of Papanastasiou (1987), described in Mitsoulis (2007) and Minatti and Paris (2015). Regularisation is required as the apparent viscosity approaches infinity at low strain rates when using equation 410, reducing the simulation time step and significantly increasing computational cost. At these high viscosities, the simulation time step approaches zero, significantly increasing computational time. Using the Papanastasiou (1987) approach, the regularised viscosity used in simulations is:

$$\hat{\eta} = \frac{\tau_y}{\dot{\gamma}}\left(1 - e^{-c\dot{\gamma}}\right) + \mu + \alpha\dot{\gamma} \quad (115)$$

where c is the viscosity scaling parameter, larger values of c result in a better approximation of the constitutive equation (equation 104), while smaller values result in smaller apparent viscosities and larger simulation time steps. Here we set cm = 200, a value which yielded the best balance between simulation speed and accuracy in validation simulations that compared comparing flow down an inclined plane with analytical solutions. from validation simulations.

Formatted: Font: Italic

Lahar simulations

Static and dynamic pressures acting on the buildings in the Quebrada Dahlia study area were determined for twelve different inundation scenarios. The scenarios were designed to explore a wide range of flow types and velocities and therefore may not represent any specific event or plausible set of events likely in Quebrada Dahlia. We use the same SPH particle spacing and terrain resolution (12.5 cm) of previous simulations by Mead et al. (2015). This resolution provided the best balance between computational time and resolution of fine scale features that can affect the flows. The scenarios were designed to explore a wide range of flow types and velocities and therefore may not represent any specific event or plausible set of events likely in Quebrada Dahlia.

Inundation scenarios were designed to explore a wide range of flow types and velocities in order to investigate the effect of rheology and velocities on flow dynamics and forces exerted on buildings. Simulations were run for three different flow types (Newtonian, hyperconcentrated streamflow and debris flow) at Simulations were run at constant flow rates of 25, 50, 75 and 100 m^3s^{-1} for three different flow types in order to determine the effect of rheology and flow velocities on flow dynamics and forces exerted on buildings.

The flow rates were chosen to produce scenarios ranging from minimal (25 m^3s^{-1}) to extreme (100 m^3s^{-1}) overbank flooding. The ratio between inertial and gravitational forces, expressed through the Froude number, was kept below 1 (subcritical flow) for each flow rate by varying the inflow area. Froude number consistency was used here as inertial and gravitational forces are dominant controls on environmental flows such as these. Flow types were selected to represent the characteristics of the most commonly occurring flows in Arequipa – flash flood, hyperconcentrated streamflow and fine-grained, matrix-supported debris flow (Thouret et al., 2013). Rheology of flash flood flows was considered to be completely Newtonian with a viscosity of water (i.e. τ_y, α = 0, μ = 0.001 and density (ρ) = 1000), rheological parameters for hyperconcentrated and debris flows (Table 23) were chosen

using the dimensionless ratio between dispersive and viscous stresses explained in Julien and Lan (1991). Values for yield strength (~~of~~ τ_y), viscosity (μ) and the turbulent-dispersive coefficient (α) were taken from the experiments of Govier et al. (1957) and Bagnold (1954), reported in Julien and Lan (1991). For a hyperconcentrated streamflow, we presumed a particle concentration by volume (C_v) of approximately 30% consisting mostly of finer particles, meaning viscous stresses are still relatively important. Debris flow scenarios were assumed to contain larger particles at a higher value C_v of approximately 55%. The particle concentration acts to increase density, viscosity and the dispersive stress coefficient in hyperconcentrated and debris flow rheologies compared to a fully Newtonian water flow. The higher particle concentration of the debris flow (compared to a hyperconcentrated flow) also results in a much higher dispersive stress coefficient, ~~. While the higher concentration increases the viscosity compared to a hyper-concentrated flow, the dispersive stress coefficient is also much higher,~~ meaning that dispersive stresses will have more importance in determining flow behaviour.

Computational cost limits the length of simulations to ~~T~~the first 45 seconds of lahar flow ~~were analysed~~ for each scenario. The flow was not established and constant by 45 seconds, so these simulations do not represent the forces exerted on buildings by a steady flow rate. Instead, the scenarios considered here are more representative of the higher velocity and depth surges or waves in a lahar. ~~While the flow was not established and constant by 45 seconds, computational cost limited simulation duration, so the scenarios considered here are more representative of the damage caused by an initial lahar surge. We expect these surges cause the most damage to buildings as they have higher velocities and depths than a steady lahar flow.~~

Flow behaviour

Figure 5 displays snapshots of velocity and dynamic pressure magnitudes for each flow type at a flow rate of 75 m^3s^{-1}. Snapshots were taken at 15-second intervals and dynamic pressure was calculated as $\rho v^2/2$, where v is the velocity magnitude. Lahars mostly followed the developed channel of Quebrada Dahlia for the first 15 seconds before overtopping the bank and spreading outwards. Channel and overbank pressures and velocity profiles are similar for Newtonian and hyperconcentrated flows, but the velocity of overbank flow is much lower for the debris flow rheology. This lower velocity is presumably caused by increased friction in the debris flow due to the higher viscosity and dispersive coefficients ~~in the debris flow~~. The dynamic pressure differs between each rheology as a result of the varied densities (and lower velocity for debris flows)~~;~~, however, the ~~The difference between Newtonian and hyper-concentrated flow velocity profiles is minimal. While there is a small yield and dispersive stress component to the hyperconcentrated rheology, the Newtonian component (i.e. the linear stress-strain relationship) still appears to be important for these flows. However, the higher density of hyperconcentrated rheologies compared to Newtonian causes an observable difference in the magnitude of dynamic pressure. Velocities are much lower for the debris flow rheology, presumably as a result of the higher dispersive coefficient. The~~ maximum pressure is still similar ~~to that of Newtonian and hyperconcentrated flows~~ between rheologies as maximum velocities are mostly confined to the channel.

The highest dynamic pressures ~~magnitudes~~ in Fig. 5 are ~~shown~~ present along the centre of the channel, with much lower pressures ~~in the vicinity of~~near the buildings. The velocity magnitude may therefore not accurately represent the pressure forces ~~Dynamic pressure may therefore not be~~ acting perpendicular to the walls of each building. The critical strength of a wall is determined from the forces acting normal (perpendicular) to the structure, therefore it is important to calculate dynamic pressure from velocity normal to the wall. The section of Quebrada Dahlia

Formatted: Highlight

studied here runs in a North-South direction and the buildings have walls that are oriented either parallel or perpendicular to the channel, so an initial understanding of the perpendicular forces acting on walls can be interpreted from the North-South (N-S) and East-West (E-W) velocity components. ~~the city blocks. The directional components of dynamic pressure are important to consider as the critical strength of a wall or building is determined from forces acting normal (perpendicular) to the structure.~~ Figure 6 shows the dynamic pressure calculated from directional velocity components ~~of dynamic pressure~~ at 40 seconds for a flow rate of 75 m^3s^{-1}. ~~The section of Quebrada Dahlia studied here runs in a North-South direction and the buildings are oriented parallel to the channel, so a broad understanding of normal pressure acting on buildings can be interpreted from the NS and EW components of pressure.~~ Figure 6 shows a consistent pattern for all rheologies ~~across the rheology range~~ where the pressure ~~magnitude~~ is dominated by the ~~pressure acting in the~~ streamwise ~~streamwise~~ (N-S) ~~direction~~velocity. The ~~perpendicular~~ pressure applied to walls facing the stream (~E-W ~~pressure~~direction, 3rd column of Fig. 6) is much lower than the pressure applied to walls perpendicular to the stream~~streamwise pressure~~. Higher ~~EW~~ pressures for EW ~~velocites~~velocities are observed along cross streets splitting each city block; however, the pressure ~~component~~ that acts ~~acting~~ perpendicular (NS) to these walls is ~~also~~ minimal. These observations indicate that ~~the~~ pressure calculated from the magnitude of velocity ~~magnitude~~, which is often assumed to be acting perpendicular to walls (e.g. Zanchetta et al., 2004; Jenkins et al., 2015), can be much higher than ~~normal~~ actual pressure acting on walls and the use of ~~pressure~~ velocity magnitudes could therefore lead to an over-estimation of building damage.

In order to accurately estimate normal forces on walls, we calculate pressures from the velocity normal to each block. The normal velocity of fluid near each block face (e.g. North and West faces of 'East 3' block) is calculated using the dot product of simulated velocity vectors and the direction vector of the block face. This normal velocity (v_n) is averaged across the face and used to calculate a 'normal' pressure using $\rho v_n^2/2$. Figure 7 compares the ~~mean~~ dynamic pressures calculated from velocity magnitude and normal velocity for ~~magnitude and the mean normal pressure acting on~~ the 'West 2' block (see Fig. 2c) ~~for various~~ atfor ~~Netwonian~~Newtonian, hyperconcentrated and debris flow types. The pressures are measured for walls oriented approximately parallel to the quebrada (labelled 'Parallel') and north facing walls that are oriented approximately perpendicular to the quebrada (labelled 'Perpendicular'). The ~~normal~~ pressures exerted on parallel walls by the normal velocity ~~are~~ up to five times lower than velocity magnitude ~~the pressure magnitude~~pressures. ~~Normal~~ The pressure applied to perpendicular walls also differs between normal velocity and magnitude, with ~~from the pressure magnitude and~~ the timing of peak ~~mean~~ pressure also ~~is a~~affected. This further ~~indicates~~ demonstrates the importance of considering normal ~~pressure~~ velocity rather than velocity magnitude w~~components w~~hen estimating dynamic pressures (and consequently damage).

~~Mean normal p~~Pressures acting on each block in the study area, calculated using the technique explained in the previous paragraph, are shown in Fig. 8 for a flow rate of 75 m^3s^{-1}. Blocks 'East 1' and 'West 1' do not have walls facing perpendicular to the flow and therefore have no pressures recorded in that orientation. The pressure for each block generally follows a similar pattern through time with a well-defined peak pressure and a lower, steady background pressure. The rise of pressure to its peak value and reduction to its background value occurs over the space of approximately 20 seconds for each block ~~and is likely the result of an initial surge of flow~~. This timeframe is too short to allow for an equalisation of hydrostatic pressure between the inside and outside of buildings, ~~suggesting~~ confirming that both hydrostatic and dynamic pressures are acting on walls during lahar surges. The

Formatted: Highlight

Formatted: Not Highlight

Formatted: Highlight

Formatted: Highlight

Formatted: Superscript

timing of the peak is delayed for downstream blocks and the magnitude of the peak for each block varies. The differences in peak pressure are caused by exposure effects such as orientation and elevation of each block relative to the quebrada. Walls facing perpendicular to the stream are generally exposed to higher dynamic pressures than parallel walls, but this effect appears to vary and could be dependent on cross-street elevations (cross-streets leading away from Qda. Dahlia increase in elevation at different rates) ~~differences~~.

In terms of rheology, hyperconcentrated flows mostly displayed the highest dynamic pressures acting on parallel walls~~blocks~~. The higher density (compared to Newtonian flows) ~~as the higher density causes~~ is responsible for the larger dynamic pressures (c.f. Jenkins et al., 2015). ~~. T~~This effect is moderated by the yield strength of the hyperconcentrated flows~~,~~ which cause the velocity ~~(and therefore pressure)~~ to be lower than Newtonian flows near perpendicular walls. Debris flow pressures are much lower than both Newtonian and hyperconcentrated flows as the yield strength and dilatant rheology components limit overbank flow velocities.~~Pressures for the debris flow are much lower than Newtonian and hyperconcentrated flows due to the yield strength and significant dilatant component that limits velocities outside of the main channel.~~

Application of critical depth-pressure curves

Depth at the maximum value of ~~mean~~ pressure acting on block walls~~long the block~~ for each scenario is used to determine if ~~the~~ individual buildings in the study area can withstand the bending moment applied by hydrostatic and dynamic pressure. Figures 9 to 11 plot the peak pressure and 'surge depth' (depth at the time of peak pressure) for Newtonian, hyperconcentrated and debris flows alongside critical depth-pressure curves for vulnerability classes A0, A and B with a ~~brick~~ wall thickness ~~width~~ of 150 mm (results for 250 mm ~~brick widths~~ wall thickness' are provided as supplementary material). The hazard variables of flow rate and lahar rheology appear to ~~have an effect on~~influence building damage, although the size of the effect is difficult to determine since most scenarios place depth and pressure combinations well above the critical curves for each block. The flow depth, which affects hydrostatic pressure and bending moment location, generally increases with the flow rate while the dynamic pressure appears to be mostly controlled by the rheology in combination with flow rate. The forces applied to the 'West 2' block, containing one class A and 4 class B buildings, are lower than the other blocks. This is possibly due to the ~~blocks~~ relative elevation and orientation of each block to the quebrada (i.e. exposure) affecting dynamic pressure and lahar depth~~fluid height~~. Debris flow scenarios at flow rates of 25, 50 and 75 m^3s^{-1} indicate depths and pressures below the critical limit for this block's building classes.

The orientation of walls to the flow direction is another element of exposure that affects the normal pressure exerted on walls. In ~~a number of~~several scenarios, perpendicular walls are subjected to higher dynamic pressures and lower depths than parallel walls. However, this e~~a~~ffect appears to be conditional to the rheology of the flow as the opposite is true for debris flow scenarios. These two effects demonstrate the importance of considering exposure elements separately to vulnerability.~~These two effects demonstrate the importance of considering exposure elements separately to vulnerability as the hazard causes the effect of vulnerability to vary.~~

The proportion of buildings with depths and pressures above the critical curve for each scenario is shown in Fig. 12 for 150 mm~~0.15 m~~ brick widths and Fig. 13 for ~~0.~~250 mm ~~brick~~ wall thicknesses~~widths~~. Assuming a binary damage state model where damage is complete for depths–pressure combinations above the curve, these proportions can be used to directly represent building loss. For the thinner ~~bricks~~walls, all class A0 buildings are above the curve for all scenarios ~~with the exception of~~apart from the 25 m^3s^{-1} debris flow. The 'East 1' block is

not inundated in this scenario, resulting in two undamaged class A0 buildings. Class A and B buildings are also mostly destroyed, with the exception of lower flow rate hyperconcentrated and debris flow scenarios where some blocks are on the edge of inundation and therefore subjected to much lower depth–pressure combinations. Slightly fewer building losses occur with larger brick widths (Fig. 13) as the larger section modulus results in a greater resistance to bending moments. However, most buildings are still destroyed in Newtonian and hyperconcentrated flow scenarios. An exception to this is the 75 m^3s^{-1} Newtonian flow where the highest pressure on the 'East 1' block occurs early in the simulation when the surge depth is low, reducing the magnitude of hydrostatic pressure and lowering the size of the applied moment.

The building loss results indicate that class A0 buildings are most vulnerable, with class A buildings marginally stronger due to the roof support. Losses for type B buildings in this area are much lower; however, this appears to be more related to building exposure than structural strength as most type B buildings ~~are located in~~are in two blocks subjected to lower depth–pressure combinations for all~~across~~ scenarios. Overall, similar to the observations in Jenkins et al. (2015), the data presented here suggests that building strength (i.e. the vulnerability component) has a minimal effect on losses, and building location (i.e. exposure) relative to flow rate and type (i.e. hazard) plays a much greater role~~(Jenkins et al., 2015) in determining loss~~.

Limitations and ~~D~~discussion

The losses shown in Figs. 12 and 13 are estimates based on several~~a number of~~ assumptions that, while necessary for the estimation of building loss, could limit the accuracy of ~~these~~ results. Firstly, the depth-pressure curves are created using ultimate bending moments derived from a foreign standard and do not consider proportional losses, only assuming ~~Losses in Figs. 12 and 13 assume~~ damage is complete for depths and pressures above the critical curve. Second, the flow scenarios modelled here are a subset of likely scenarios and do not ~~model~~replicate all damage causing actions of lahar flow. Finally, the maximum total pressure was assumed to be the sum of hydrostatic and dynamic pressure and to occur when dynamic pressure was at its peak. These limitations are discussed and justified in this section to highlight areas of improvement necessary for robust, quantitative estimation of lahar damage and vulnerability.

Depth-pressure curves

Formatted: Heading 2

T ~~T~~he critical depth-pressure curve is the contour where the ratio of applied (pressure) moment equals the ultimate (failure) moment of a given masonry wall. The calculation of ultimate bending moments followed an Australian standard (AS3700-2011). Although bending moment calculations are similar for all national standards and material properties from Arequipa were used as inputs, the standard inherently assumes conformance to construction and design standards. This is demonstrated through the assumption of a minimum mortar strength of 0.2 MPa. Page (1996)~~Page (1996)~~ suggests this strength can be achieved with correct mortar composition (Page, 1996)and laying.; however, lower strengths are possible if there is low conformance to design standards. The makeshift structures that characterise class A0 buildings are likely to have mortar bond strengths much lower than the implied minimum of 0.2 MPa. This mischaracterisation of mortar strengths for makeshift structures will result in an over-estimation of building strength and critical-depth pressure curves. Additionally, the depth-pressure

Formatted: Highlight

curves assume a binary damage state, where failure is total when the applied (pressure) moment equals the ultimate (failure) moment. This neglects incremental damage states that require building repair (e.g. to doors or windows) and can cause a reduction in the overall building strength.

~~Both of these~~Both of these assumptions will result in an under-estimation of loss if violated. Most of the flow scenarios caused depths and pressures that exceeded critical curves by a large margin and resulted in an almost total loss; conversely, flow scenarios that did not result in total or near-total losses usually had depths and pressure values that were well below the critical curves. This suggests that these assumptions are not critical to the results shown here, but~~y~~ may be important to consider in other case study areas.

Flow scenarios

The twelve flow scenarios were chosen to understand the effect of hazard properties (flow rate and rheology) on total loss. These scenarios may not represent any specific lahar event for Qda. Dahlia. Rather, scenarios were chosen to be representative of the range of lahar rheologies and flow rates that can cause building damage in Arequipa. The chosen flows have similar characteristics to observed lahars and lahar deposits (Thouret et al., 2013) and are therefore reasonably representative of the lahar hazards expected in Arequipa.

However, damage caused by these hazards may not be representative as ~~-~~only the direct actions of hydrostatic and dynamic pressure were considered in this study.

~~Given that only direct actions are considered in this study, the curves likely form an upper bound to complete damage and depth–pressure combinations below the curve may still result in building damage through other mechanisms.~~ While direct actions are regarded as the most important source of damage, they are also favoured in risk assessment due to the large scale predictability of hydrostatic and dynamic forces (Kelman and Spence, 2004). Damage is likely to also be caused by scour and large debris missiles within the flow (Jenkins et al., 2015). In particular, boulders are often carried by lahars at the flow front (Iverson, 1997; Doyle et al., 2011) and can lead to significant damage (e.g. Zeng et al., 2015). However; these actions are harder to predict and incorporate into large scale loss analyses (Kelman and Spence, 2004). These unstudied actions are generally proportional to depth, pressure or velocity, indicating that there may be a relationship between the ratio of applied to ultimate moment and damage through other actions.

Given that only direct actions are considered in this study, the curves likely form an upper bound to complete damage, and depth–pressure combinations below the curve may still result in complete building damage through other mechanisms. ~~However, comprehensive data on loss events would be required to accurately refine the damage state model into several different damage states that consider the effect of other actions.~~

Pressure actions

~~Pressure surges observed in the simulation occurred over too short a duration to allow for equalisation of hydrostatic pressure between the inside and outside of buildings. As a result, b~~Both hydrostatic and dynamic pressures were considered in bending moment calculations. ~~S~~Slower increases in depth, ~~ or~~ buildings with ~~a large number of~~many openings and the location of buildings relative to the channel can ~~could result i~~also affect the ~~n~~

Formatted: Heading 2

Formatted: Heading 2

an eequalisation of ~~water~~ lahar depths and reduce~~cause~~ the effect of hydrostatic pressure~~ to be negligible~~. However, lahar depth would still be an important factor to consider in building damage estimation as it ~~still~~ controls location of the bending moment and can cause damage through other actions (e.g. inundation damage, buoyancy, corrosion).

The applied depth at the time of maximum pressure was used here to create the depth-pressure combinations to determine building loss. This 'surge depth' was not necessarily the maximum depth of the lahar during the simulation. Maximum depths generally occurred at later times in the simulations when hydrostatic pressure may have equalised inside and outside buildings. This assumption of 'surge depth' was valid for most cases, although the losses for the 75 m^3s^{-1} Newtonian flows indicate that this approach can be too simplistic at times. The complexity of lahar flows within urban environments with intricate geometry and obstacles similar to the case study area means that broad generalisations and assumptions about flow dynamics, such as the assumption of a 'surge depth', are often limited in their validity.

Discussion

The combination of pressures applied to each block in the study area created bending moments that, with few exceptions, were much higher than the maximum moment buildings could withstand. The limitations identified in previous sections generally over-estimate building strength and resilience to lahars which would result in greater damage than predicted here. The estimated building losses (Figs. 12 and 13) therefore represent the minimum expected losses for each flow scenario with damage likely to be more severe due to additional damage actions (e.g. boulders impacting structures) and the over-estimation of building quality, particularly for class A0 buildings.

When inundated, blocks in this study area are subjected to depths and pressures higher than the strongest structural class buildings can withstand. Specific improvements to reduce vulnerability, such as adding roof support and utilising reinforced frames comprised of equally spaced RC columns will increase the overall strength of buildings by reducing the slenderness ratio (equation A6). Wider masonry units (~~brick~~wall thickness~~, width~~) and stronger mortar joints will also increase the overall building strength by increasing wall stiffness and therefore resistance to bending moments. However, this increased structural strength appears to only reduce losses in very low flow rate scenarios where there is proportionally less inundation. This suggests that while each component of risk has a role in determining overall building losses, the variability in individual losses appears to be predominantly caused by flow dynamics (i.e. lahar hazard) and building exposure (e.g. proportion of building types and orientation within blocks).

~~The building type, flow rate and flow type appear to have a large effect on overall building losses (Figs. 12 and 13); however, the variability in individual building losses appears to be predominantly caused by flow dynamics and building exposure (e.g. proportion of building types and orientation within blocks)~~ ~~. This suggests that urban flow environments may be too complicated to directly estimate flow behaviour from observed building losses.~~

Formatted: Heading 2

Formatted: Not Highlight

Formatted: Not Highlight

Formatted: Not Highlight

Conclusion

Development of fragility functions in the form of critical depth-pressure curves for building classes within Arequipa have helped to provide insight into possible building losses and their cause. Building vulnerability is largely controlled by social, cultural and institutional factors (Künzler et al., 2012), so the depth-pressure curves are necessarily specific to Arequipa building typologies. However, given sufficient data on building strength, depth-pressure curves can be generated through the same approach as in Appendix A and used to ~~-~~quantify masonry building loss in terms of flow depth and pressure in other ~~areas~~regions.

~~The e~~Estimated building losses (Figs. 12 and 13) are caused by the intersection of lahar hazard (flow rate, flow type) with building exposure (location, proportion of building types and orientation within blocks) and vulnerability (building type and strength). The almost total simulated building loss for all scenarios indicates that ~~that the quality of buildings is insufficient in this area and that~~ substantial losses can be expected in the event of inundation. Furthermore, lahar depths and pressures obtained from simulations were much greater than those most buildings in the study area could withstand, even if retrofitting to improve structural strength was undertaken. This suggests that, in this study area at least, exposure and lahar hazard have a larger role in determining building loss compared to vulnerability. ~~As inundation level is controlled by lahar volume, rheology and building exposure, these factors are therefore the most important in determining damage in this study area. Vulnerability can be decreased by increasing the structural strength of buildings through retrofitting building structures to improve quality. Specific improvements such as adding roof support and utilising reinforced frames comprised of equally spaced RC columns will increase the overall strength of buildings by reducing the slenderness ratio (equation 6). Wider masonry units (brick width) and stronger mortar joints will also increase the overall building strength by increasing wall stiffness and therefore resistance to bending moments. However, the increased structural strength appears to only reduce losses in very low flow rate scenarios where there is proportionally less inundation.~~

~~The approach demonstrated here, while focusing on building typologies in Arequipa, can be generalised to quantify masonry building loss in terms of flow depth and pressure in other areas. However, sufficient data on building strength is often not readily available on a large scale and demonstrates the need for focused studies in high risk areas affected by lahars. This also highlights the complementary relationship between large-scale vulnerability indices and direct vulnerability-damage relationships. Large-scale indicators of vulnerability can locate areas in need of focused study and loss analysis. Detailed modelling of vulnerability, shown here, can be used in turn to refine the indices in order to focus on the most relevant indicators of damage.~~

Appendix A. Calculating ultimate bending moment and shear force

Formatted: Heading 1

The ultimate bending moment (M_u) and ultimate shear force (V_u) is calculated using the following equations (Roos, 2003):

$$M_u = (f_t + f_d)\frac{wb^2}{6} \quad \text{(A1)}$$

$$V_u = f_v wb \quad \text{(A2)}$$

where f_t is the tensile strength of the masonry wall, f_d is the design compressive stress acting on the wall, w is the width of the wall facing the flow and b is the thickness of the wall. The shear strength of the masonry wall (f_v) is related to the tensile and compressive stress through (Roos, 2003):

$$f_v = 0.5f_t + 0.5f_d \quad \text{(A3)}$$

Formatted: Right

The tensile strength is assumed to be 0.2 MPa as, according to AS3700-2011, the tensile strength should be no greater than this value without testing.. The wall thickness, b, is between 150 and 250 mm for terracotta bricks (Martelli, 2011) and is assumed to be similar for ignimbrite bricks observed in the study area. The design compressive stress, f_d, can be determined by calculating the vertical forces (i.e. building weight) acting on the walls. This can be estimated from building properties such as number and weight of floors, weight of the masonry and building design (e.g. Roos, 2003). However, such detailed building data is lacking here and carries considerable uncertainty for a heterogeneous urban area with varied construction materials, building ages and designs such as Arequipa. Instead we use the design compressive capacity (f_o), specified in AS3700-2011, to determine the design compressive stress:

$$f_o = \phi f_c A_b \quad \text{(A2)}$$

$$f_d = k f_o \quad \text{(A3)}$$

where f_c is the characteristic compressive strength of the masonry, ϕ is the capacity reduction factor, A_b is the bedded area of the masonry (brick width × length) and k is a reduction factor based on the wall design. The characteristic compressive strength is determined using the unconfined compressive strength tests of Martelli (2011) on building materials sourced from Arequipa. Presuming the mortar is of relatively low quality (M2), the characteristic compressive strengths (according to AS3700-2011) are 3.8 MPa for ignimbrite masonry and between 3.5 and 4.54 MPa for terracotta masonry. The slenderness reduction factor, k, describes the susceptibility to buckling. Following AS3700-2011, this factor is calculated as

$$k = 0.67 - 0.02(S_{rs} - 14) \quad \text{(A4)}$$

for buildings with a reinforced concrete roof or floor (i.e. typologies 3-6C), and

$$k = 0.67 - 0.025(S_{rs} - 10) \quad \text{(A5)}$$

for buildings with other roof or floor supports (typologies 1-2). This factor requires a calculation of the slenderness ratio, S_{rs}:

$$S_{rs} = \frac{a_v H}{k_t b} \quad \text{(A6)}$$

where H is the height between floors or supports, taken as 2.8 metres for reinforced concrete type buildings and 3 metres for non-reinforced buildings (Martelli, 2011). The vertical slenderness coefficient, a_v, is determined from the lateral support along the top edge of the wall. Walls with roof support (types 3-6~~C~~) have a coefficient of 1, while unsupported walls (types 1A-2B) act as a cantilever and have a coefficient of 2.5. Considering the thinnest bricks, the slenderness coefficient is negative for building types 1A-2B as the design is out of the range of those considered in AS3700-2011. Acknowledging the low strength of these frequently makeshift structures, the slenderness coefficient is therefore set to 0.01. The thickness coefficient, k_t, takes into account the strength of supporting columns. This coefficient is set to 1 for non-reinforced frame buildings and is dependent on the spacing and thickness of reinforced beams within the masonry for reinforced buildings. Estimates of the spacing and thickness suggest that the coefficient will be between 1.4 and 2 for type 6A-6C buildings and between 1 and 1.2 for type 4 buildings. The large spacing between reinforced columns and their relative width, pictured in Thouret et al. (2014), are responsible for the much lower coefficients assigned to type 4 buildings.

Formatted: Normal

~~Roos (2003)~~**Acknowledgements**

The authors would like to thank the Civil Defence office in Arequipa (Instituto Nacional de Defensa Civil INDECI), in particular the Regional office (Mrs A. Arguedas) and the Provincial/City office (Mr. J. Vasquez) for support during field work as well as the students of the department of geology of the University Nacional San Aguistin in Arequipa. JCT's work in Arequipa has been supported by the Labex CLERVOLC (contribution number ~~XXX~~235), the PICS CNRS program and the French Embassy in Lima.

References

Auker, M., Sparks, R., Siebert, L., Crosweller, H., and Ewert, J.: A statistical analysis of the global historical volcanic fatalities record, J Appl. Volcanol., 2, 1-24, 10.1186/2191-5040-2-2, 2013.

Bagnold, R. A.: Experiments on a gravity-free dispersion of large solid spheres in a Newtonian fluid under shear, Proceedings of the Royal Society of London A: Mathematical, Physical and Engineering Sciences, 1954, 49-63,

Cleary, P., Prakash, M., Mead, S., Lemiale, V., Robinson, G., Ye, F., Ouyang, S., and Tang, X.: A scenario-based risk framework for determining consequences of different failure modes of earth dams, Natural Hazards, 75, 1489-1530, 10.1007/s11069-014-1379-x, 2015.

Cleary, P. W., and Prakash, M.: Discrete–element modelling and smoothed particle hydrodynamics: potential in the environmental sciences, Philosophical Transactions of the Royal Society of London. Series A: Mathematical, Physical and Engineering Sciences, 362, 2003-2030, 10.1098/rsta.2004.1428, 2004.

Cleary, P. W., Prakash, M., Mead, S., Tang, X., Wang, H., and Ouyang, S.: Dynamic simulation of dam-break scenarios for risk analysis and disaster management, International Journal of Image and Data Fusion, 3, 333-363, 2012.

Custer, R., and Nishijima, K.: Flood vulnerability assessment of residential buildings by explicit damage process modelling, Natural Hazards, 78, 461-496, 10.1007/s11069-015-1725-7, 2015.

de Bélizal, E., Lavigne, F., Hadmoko, D. S., Degeai, J.-P., Dipayana, G. A., Mutaqin, B. W., Marfai, M. A., Coquet, M., Mauff, B. L., Robin, A.-K., Vidal, C., Cholik, N., and Aisyah, N.: Rain-triggered lahars following the 2010 eruption of Merapi volcano, Indonesia: A major risk, Journal of Volcanology and Geothermal Research, 10.1016/j.jvolgeores.2013.01.010, 2013.

Di Baldassarre, G., and Montanari, A.: Uncertainty in river discharge observations: a quantitative analysis, Hydrol. Earth Syst. Sci., 13, 913-921, 10.5194/hess-13-913-2009, 2009.

Doyle, E. E., Cronin, S. J., Cole, S. E., and Thouret, J. C.: The coalescence and organization of lahars at Semeru volcano, Indonesia, Bulletin of Volcanology, 72, 961-970, 10.1007/s00445-010-0381-8, 2010.

Doyle, E. E., Cronin, S. J., and Thouret, J. C.: Defining conditions for bulking and debulking in lahars, Geological Society of America Bulletin, 123, 1234-1246, 10.1130/B30227.1, 2011.

Dumaisnil, C., Thouret, J. C., Chambon, G., Doyle, E. E., Cronin, S. J., and Surono: Hydraulic, physical and rheological characteristics of rain - triggered lahars at Semeru volcano, Indonesia, Earth Surface Processes and Landforms, 35, 1573-1590, 10.1002/esp.2003, 2010.

Ettinger, S., Mounaud, L., Magill, C., Yao-Lafourcade, A.-F., Thouret, J.-C., Manville, V., Negulescu, C., Zuccaro, G., De Gregorio, D., Nardone, S., Uchuchoque, J. A. L., Arguedas, A., Macedo, L., and Manrique Llerena, N.: Building vulnerability to hydro-geomorphic hazards: Estimating damage probability from qualitative vulnerability assessment using logistic regression, Journal of Hydrology, 10.1016/j.jhydrol.2015.04.017, 2015.

Formatted: Heading 1

Galderisi, A., Bonadonna, C., Delmonaco, G., Ferrara, F., Menoni, S., Ceudech, A., Biass, S., Frischknecht, C., Manzella, I., Minucci, G., and Gregg, C.: Vulnerability Assessment and Risk Mitigation: The Case of Vulcano Island, Italy, in: Landslide Science and Practice, edited by: Margottini, C., Canuti, P., and Sassa, K., Springer Berlin Heidelberg, 55-64, 2013.

Govier, G., Shook, C., and Lilge, E.: The rheological properties of water suspensions of finely subdivided magnetite, galena and ferrosilicon, Trans. Can. IMM, 60, 147-154, 1957.

Iverson, R. M.: The physics of debris flows, Reviews of Geophysics, 35, 245-296, 10.1029/97RG00426, 1997.

Iverson, R. M., Schilling, S. P., and Vallance, J. W.: Objective delineation of lahar-inundation hazard zones, Geological Society of America Bulletin, 110, 972-984, 10.1130/0016-7606(1998)110<0972:odolih>2.3.co;2, 1998.

Jan, C.-D., and Shen, H.: Review dynamic modeling of debris flows, in: Recent Developments on Debris Flows, edited by: Armanini, A., and Michiue, M., Lecture Notes in Earth Sciences, Springer Berlin Heidelberg, 93-116, 1997.

Jenkins, S., Phillips, J., Price, R., Feloy, K., Baxter, P., Hadmoko, D., and de Bélizal, E.: Developing building-damage scales for lahars: application to Merapi volcano, Indonesia, Bulletin of Volcanology, 77, 1-17, 10.1007/s00445-015-0961-8, 2015.

Julien, P., and Lan, Y.: Rheology of Hyperconcentrations, Journal of Hydraulic Engineering, 117, 346-353, 10.1061/(ASCE)0733-9429(1991)117:3(346), 1991.

Kelman, I., and Spence, R.: An overview of flood actions on buildings, Engineering Geology, 73, 297-309, 10.1016/j.enggeo.2004.01.010, 2004.

Künzler, M., Huggel, C., and Ramírez, J. M.: A risk analysis for floods and lahars: case study in the Cordillera Central of Colombia, Natural Hazards, 64, 767-796, 10.1007/s11069-012-0271-9, 2012.

Lavigne, F.: Lahar hazard micro-zonation and risk assessment in Yogyakarta city, Indonesia, GeoJournal, 49, 173-183, 10.1023/A:1007035612681, 1999.

Manville, V., Major, J. J., and Fagents, S. A.: Modeling lahar behaviour and hazards, in: Modeling volcanic processes : the physics and mathematics of volcanism, edited by: Fagents, S. A., Gregg, T. K. P., and Lopes, R. M. C., Cambridge University Press, Cambridge, x, 421 pages, 2013.

Martelli, K.: The physical vulnerability of urban areas facing the threat of inundation from lahars and flash floods: application to the case study of Arequipa, Peru, Université Blaise Pascal-Clermont-Ferrand II, 2011.

Mead, S., Prakash, M., Magill, C., Bolger, M., and Thouret, J.-C.: A Distributed Computing Workflow for Modelling Environmental Flows in Complex Terrain, in: Environmental Software Systems. Infrastructures, Services and Applications, edited by: Denzer, R., Argent, R., Schimak, G., and Hřebíček, J., IFIP Advances in Information and Communication Technology, Springer International Publishing, 321-332, 2015.

Minatti, L., and Paris, E.: A SPH model for the simulation of free surface granular flows in a dense regime, Applied Mathematical Modelling, 39, 363-382, 10.1016/j.apm.2014.05.034, 2015.

Mitsoulis, E.: Flows of viscoplastic materials: models and computations, Rheology Reviews, 135-178, 2007.

O'Brien, J., and Julien, P.: Laboratory Analysis of Mudflow Properties, Journal of Hydraulic Engineering, 114, 877-887, doi:10.1061/(ASCE)0733-9429(1988)114:8(877), 1988.

O'Brien, J., Julien, P., and Fullerton, W.: Two ‐ Dimensional Water Flood and Mudflow Simulation, Journal of Hydraulic Engineering, 119, 244-261, doi:10.1061/(ASCE)0733-9429(1993)119:2(244), 1993.

Page, A. W.: Unreinforced masonry structures-an Australian overview, Bulletin of the New Zealand national society for earthquake engineering, 29, 242-255, 1996.

Papanastasiou, T. C.: Flows of Materials with Yield, Journal of Rheology, 31, 385-404, 10.1122/1.549926, 1987.
Patra, A. K., Bauer, A. C., Nichita, C. C., Pitman, E. B., Sheridan, M. F., Bursik, M., Rupp, B., Webber, A., Stinton, A. J., Namikawa, L. M., and Renschler, C. S.: Parallel adaptive numerical simulation of dry avalanches over natural terrain, Journal of Volcanology and Geothermal Research, 139, 1-21, 10.1016/j.jvolgeores.2004.06.014, 2005.
Phillips, C. J., and Davies, T. R. H.: Determining rheological parameters of debris flow material, Geomorphology, 4, 101-110, 10.1016/0169-555X(91)90022-3, 1991.
Pierson, T. C., and Costa, J. E.: A rheologic classification of subaerial sediment-water flows, Debris flows/avalanches: process, recognition, and mitigation, 7, 1, 1987.
Pierson, T. C.: Hyperconcentrated flow—transitional process between water flow and debris flow, in: Debris-flow hazards and related phenomena, edited by: Jakob, M., and Hungr, O., Springer, 159-202, 2005.
Pierson, T. C., Major, J. J., Amigo, Á., and Moreno, H.: Acute sedimentation response to rainfall following the explosive phase of the 2008–2009 eruption of Chaitén volcano, Chile, Bulletin of Volcanology, 75, 1-17, 10.1007/s00445-013-0723-4, 2013.
Pitman, E. B., and Le, L.: A two-fluid model for avalanche and debris flows, 1832, 1573-1601 pp., 2005.
Prakash, M., Rothauge, K., and Cleary, P. W.: Modelling the impact of dam failure scenarios on flood inundation using SPH, Applied Mathematical Modelling, 10.1016/j.apm.2014.03.011, 2014.
Rodriguez-Paz, M. X., and Bonet, J.: A corrected smooth particle hydrodynamics method for the simulation of debris flows, Numerical Methods for Partial Differential Equations, 20, 140-163, 10.1002/num.10083, 2004.
Roos, W.: Damage to buildings, Delft Cluster, 2003.
Sandri, L., Thouret, J.-C., Constantinescu, R., Biass, S., and Tonini, R.: Long-term multi-hazard assessment for El Misti volcano (Peru), Bulletin of Volcanology, 76, 1-26, 10.1007/s00445-013-0771-9, 2014.
Thouret, J.-C., Enjolras, G., Martelli, K., Santoni, O., Luque, J., Nagata, M., Arguedas, A., and Macedo, L.: Combining criteria for delineating lahar-and flash-flood-prone hazard and risk zones for the city of Arequipa, Peru, Natural Hazards and Earth System Sciences, 13, 339-360, 10.5194/nhess-13-339-2013, 2013.
Thouret, J.-C., Ettinger, S., Guitton, M., Santoni, O., Magill, C., Martelli, K., Zuccaro, G., Revilla, V., Charca, J., and Arguedas, A.: Assessing physical vulnerability in large cities exposed to flash floods and debris flows: the case of Arequipa (Peru), Natural Hazards, 73, 1771-1815, 10.1007/s11069-014-1172-x, 2014.
Toyos, G., Gunasekera, R., Zanchetta, G., Oppenheimer, C., Sulpizio, R., Favalli, M., and Pareschi, M. T.: GIS-assisted modelling for debris flow hazard assessment based on the events of May 1998 in the area of Sarno, Southern Italy: II. Velocity and dynamic pressure, Earth Surface Processes and Landforms, 33, 1693-1708, 10.1002/esp.1640, 2008.
Vallance, J. W., and Iverson, R. M.: Lahars and Their Deposits, in: The Encyclopedia of Volcanoes (Second Edition), Sigurdsson, Haraldur, Academic Press, Amsterdam, 649-664, 2015.
van Westen, C. J., van Asch, T. W. J., and Soeters, R.: Landslide hazard and risk zonation—why is it still so difficult?, Bull Eng Geol Environ, 65, 167-184, 10.1007/s10064-005-0023-0, 2006.
Vargas Franco, R., Thouret, J., Delaite, G., Van Westen, C., Sheridan, M., Siebe, C., Mariño, J., Souriot, T., and Stinton, A.: Mapping and assessing volcanic and flood hazards and risks, with emphasis on lahars, in Arequipa, Peru, Stratigraphy and Geology of Volcanic Areas, 464, 265, 2010.

Varnes, D. J.: Landslide hazard zonation: a review of principles and practice, Natural Hazards, Paris, France, 1984.

Zanchetta, G., Sulpizio, R., Pareschi, M. T., Leoni, F. M., and Santacroce, R.: Characteristics of May 5–6, 1998 volcaniclastic debris flows in the Sarno area (Campania, southern Italy): relationships to structural damage and hazard zonation, Journal of Volcanology and Geothermal Research, 133, 377-393, 10.1016/S0377-0273(03)00409-8, 2004.

Zeng, C., Cui, P., Su, Z., Lei, Y., and Chen, R.: Failure modes of reinforced concrete columns of buildings under debris flow impact, Landslides, 12, 561-571, 10.1007/s10346-014-0490-0, 2015.

Zheng, K., Sun, Z.-c., Sun, J.-w., Zhang, Z.-m., Yang, G.-p., and Zhou, F.: Numerical simulations of water wave dynamics based on SPH methods, Journal of Hydrodynamics, Ser. B, 21, 843-850, Doi: 10.1016/s1001-6058(08)60221-8, 2009.

Zuccaro, G., Cacace, F., Spence, R. J. S., and Baxter, P. J.: Impact of explosive eruption scenarios at Vesuvius, Journal of Volcanology and Geothermal Research, 178, 416-453, 10.1016/j.jvolgeores.2008.01.005, 2008.

Figures

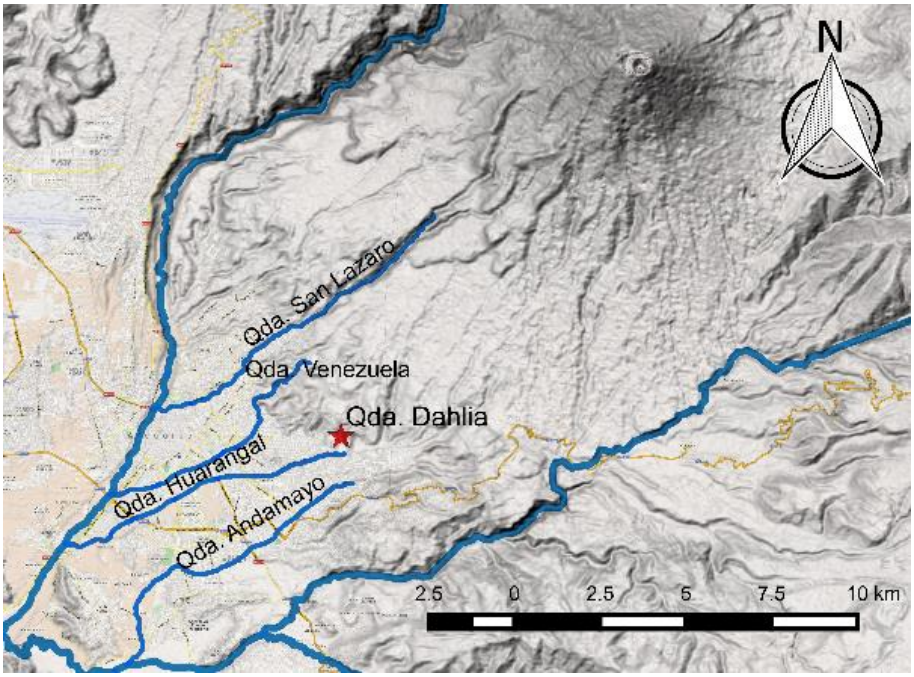
N
Qda. San Lazaro
Qda. Venezuela
Qda. Dahlia
Qda. Huarangal
Qda. Andamayo
2.5
0
2.5
5
7.5
10 km

775

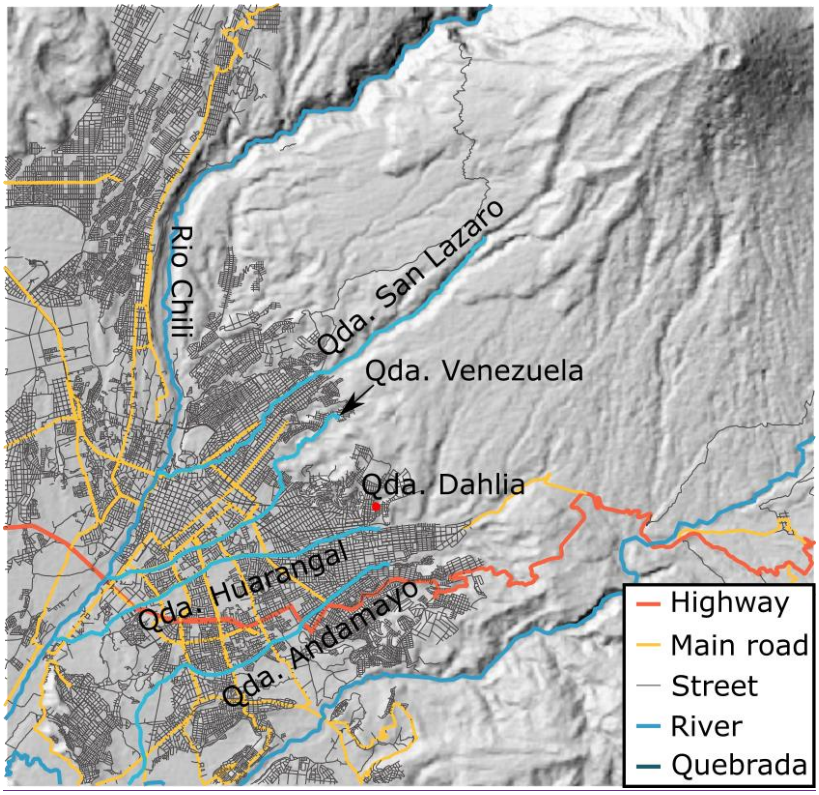

Figure 1. Location of Arequipa in relation to El Misti volcano, showing the main quebradas and the location of the Quebrada Dahlia study area.

780

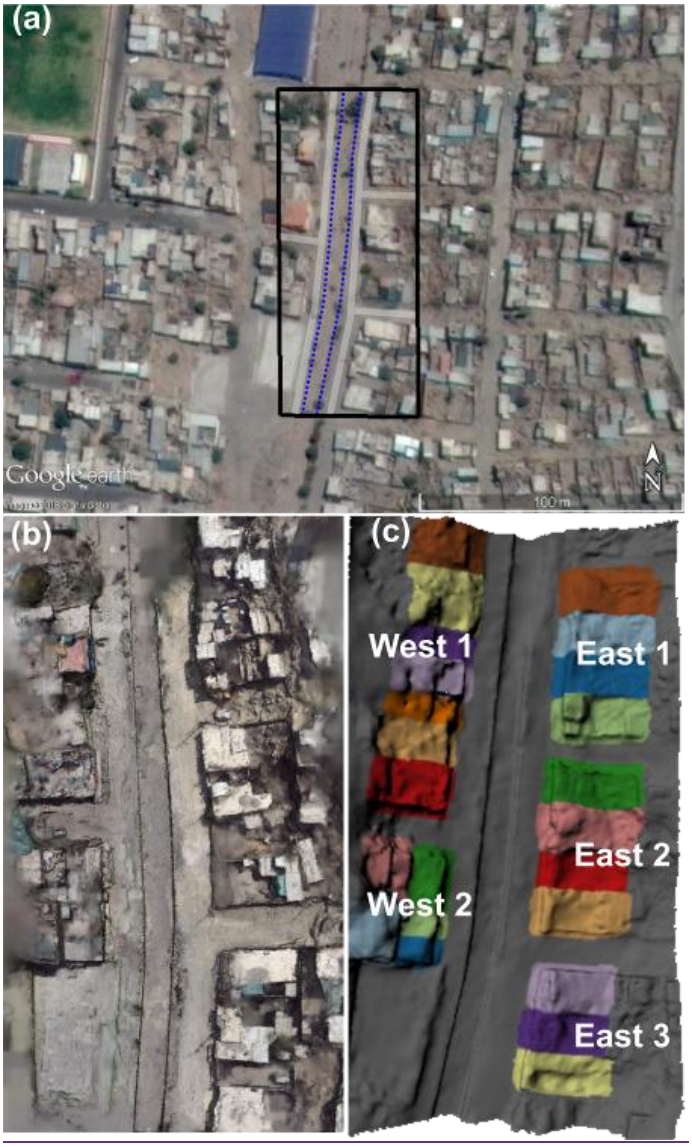
(a)
Google earth
100 m
N
(b)
(c)
West 1
East 1
East 2
West 2
East 3

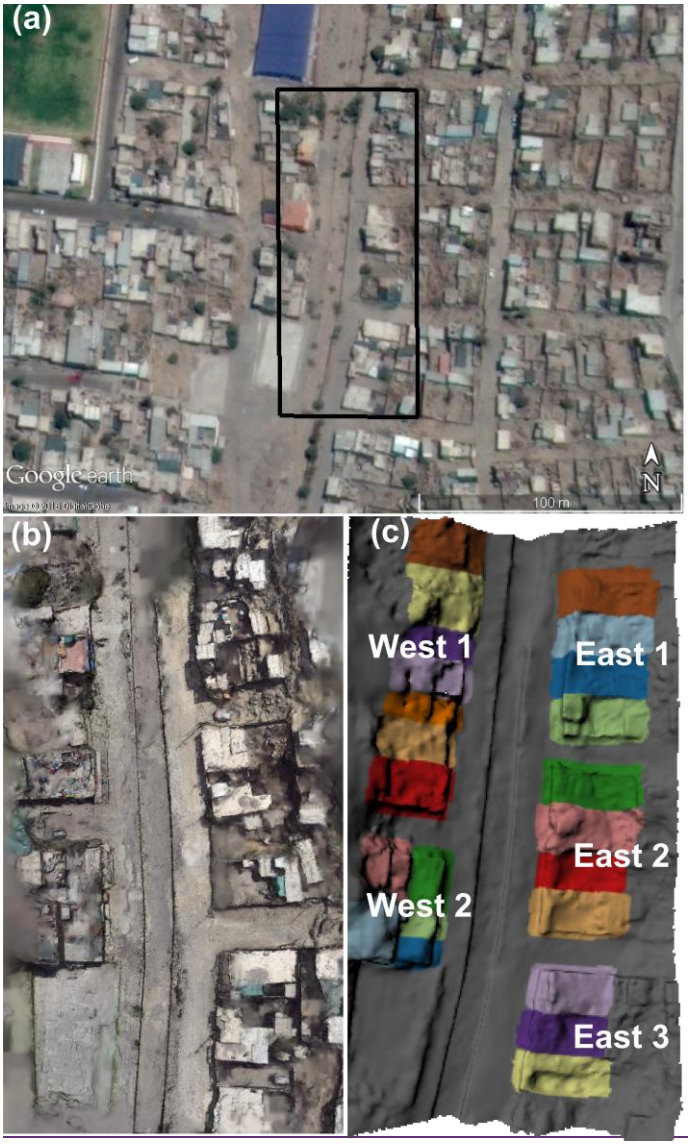

Figure 2. Overview of Quebrada Dahlia study area, Arequipa, (a) aerial image with black outline showing study area, dashed outline showing channel banks and transparent lines showing streets in the area, (b) photogrammetric reconstruction of the surface and (c) individual buildings and building blocks identified from building surveys.

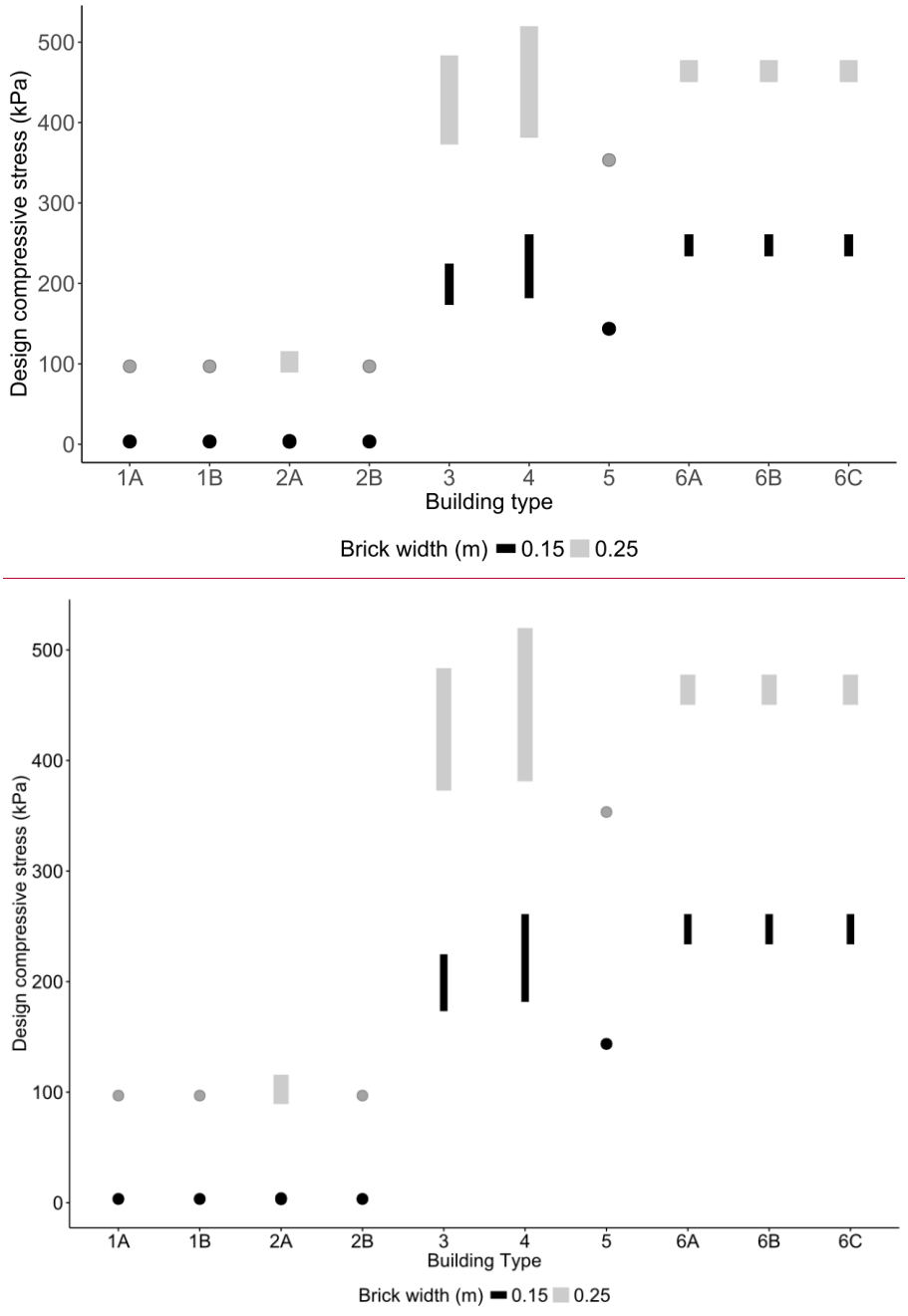

790

Figure 3. Range of design compressive stress for building types 1A - 6C defined in Thouret et al. (2014). Compressive

stress capacity was calculated for every configuration of compressive strength (f_c), bedded area (A_b), and thickness coefficient (k_t) at brick widths (b) of 150 mm and 250 mm.

795

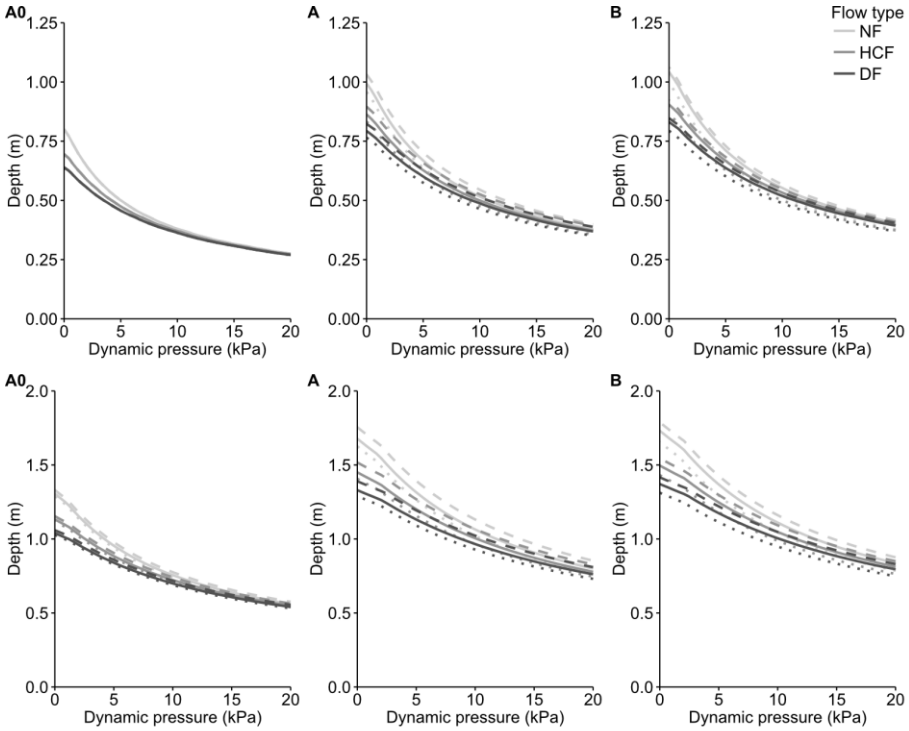
A0
A
B
Flow type
NF
HCF
DF
Depth (m)
Dynamic pressure (kPa)
0.00
0.25
0.50
0.75
1.00
1.25
0.0
0.5
1.0
1.5
2.0
0
5
10
15
20

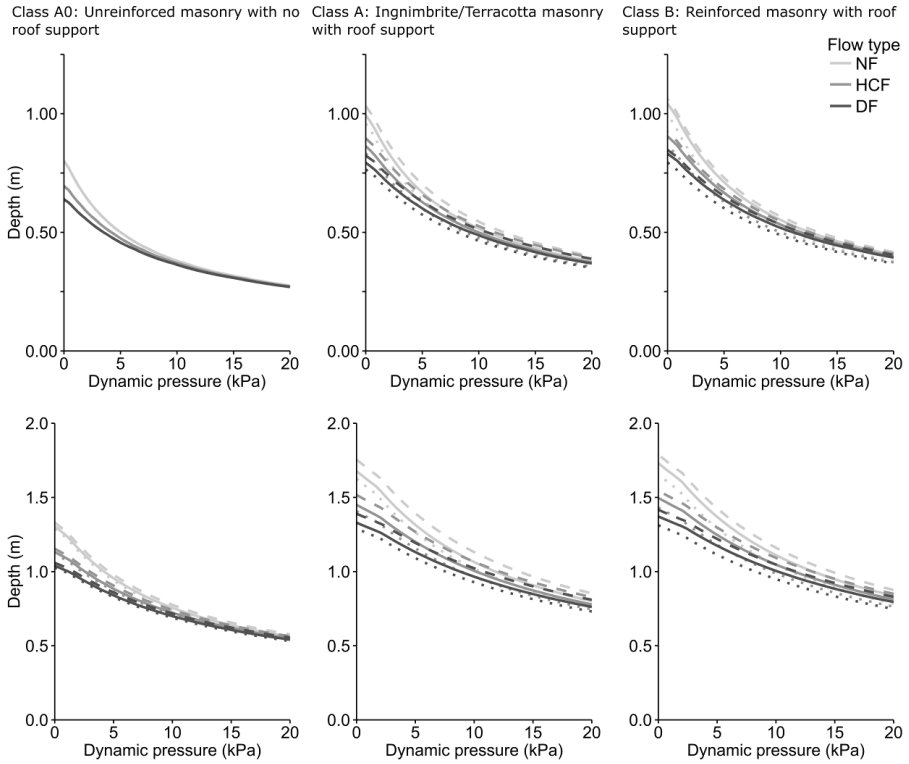

Figure 4. Critical depth and dynamic pressures for failure of ~~building~~ structural classes A0, A and B for brick widths of 0.15 m (top) and 0.25 m (bottom). Shading of the lines indicate flow type and density, dotted lines and dashed lines represent the minimum and maximum forces required. Densities are for a Newtonian flow (NF, ρ = 1000 kg·m^{-3}), hyper-concentrated flow (HCF, ρ = 1500 kg·m^{-3}) and debris flow (DF, ρ = 1915 kg·m^{-3}).

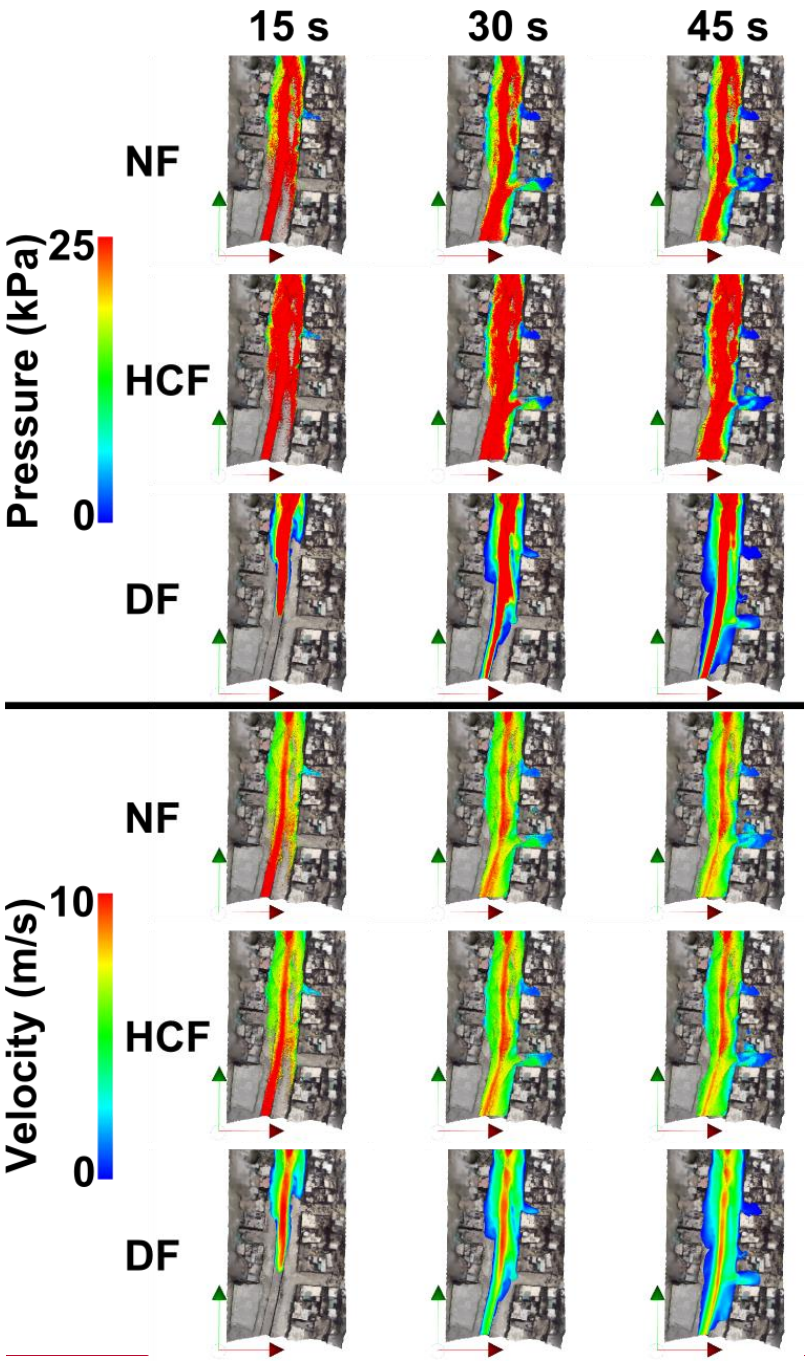
15 s
30 s
45 s
NF
HCF
DF
Pressure (kPa)
25
0
NF
HCF
DF
Velocity (m/s)
10
0

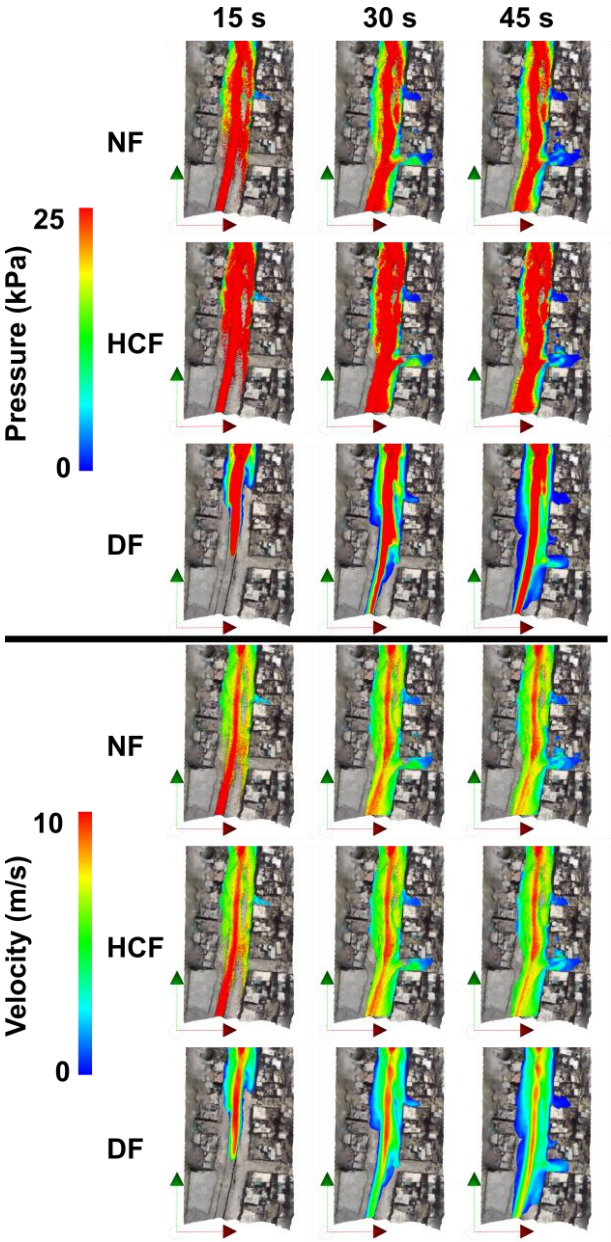

805

Figure 5. Evolution of dynamic pressure and velocity magnitudes for a 75 m^3s^{-1} flow along Quebrada Dahlia for a Newtonian flow (NF), hyperconcentrated flow (HCF) and debris flow (DF). Arrows indicate North (green) and East (red) direction.

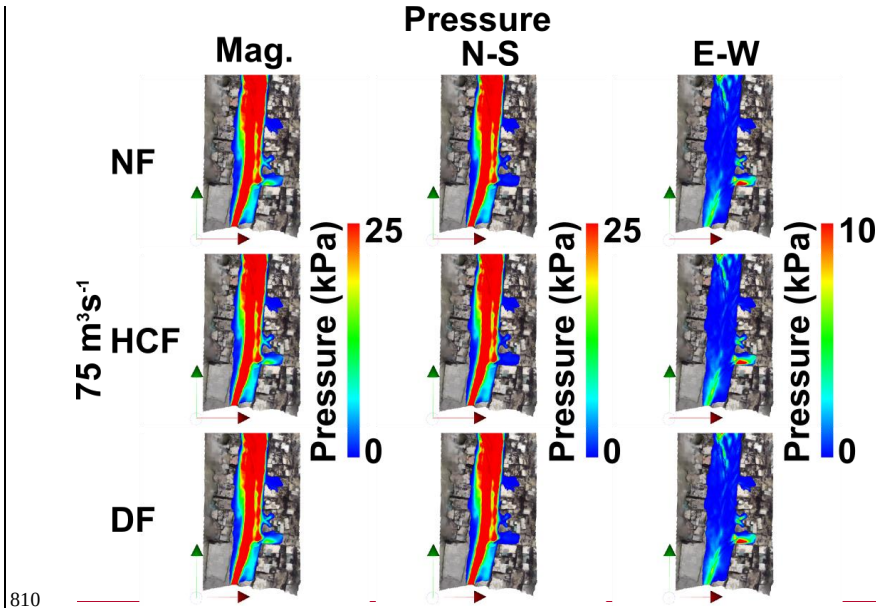
Mag.
Pressure
N-S
E-W
NF
HCF
DF
75 m³s⁻¹
Pressure (kPa)
25
0
Pressure (kPa)
25
0
Pressure (kPa)
10
0

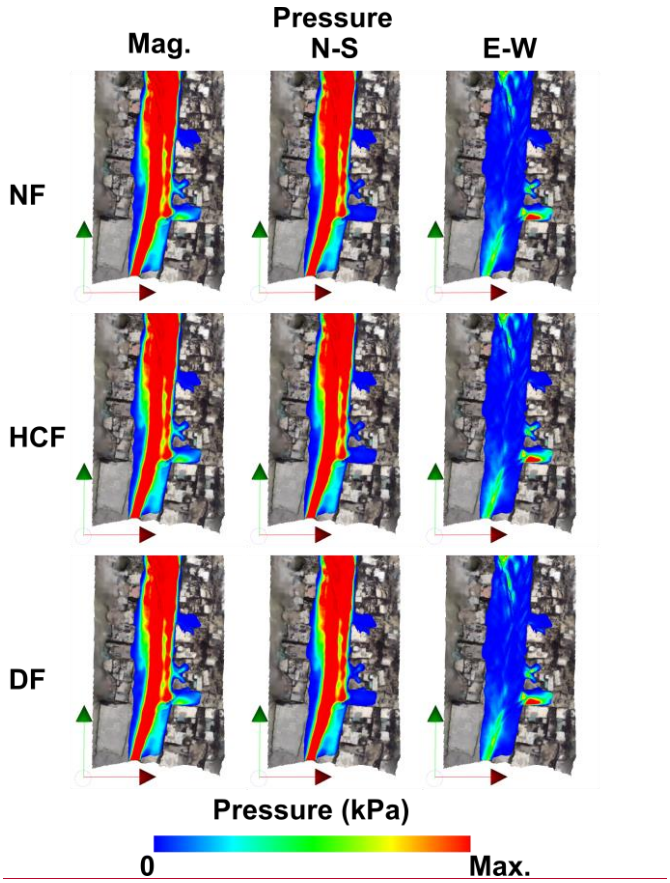

Figure 6. Directional components of dynamic pressure for a 75 m^3s^{-1} flow along Quebrada Dahlia for a Newtonian flow (NF), hyperconcentrated flow (HCF) and debris flow (DF). Maximum pressure is 25 kPa for magnitude and N-S pressures, 10 kPa for E-W pressure.

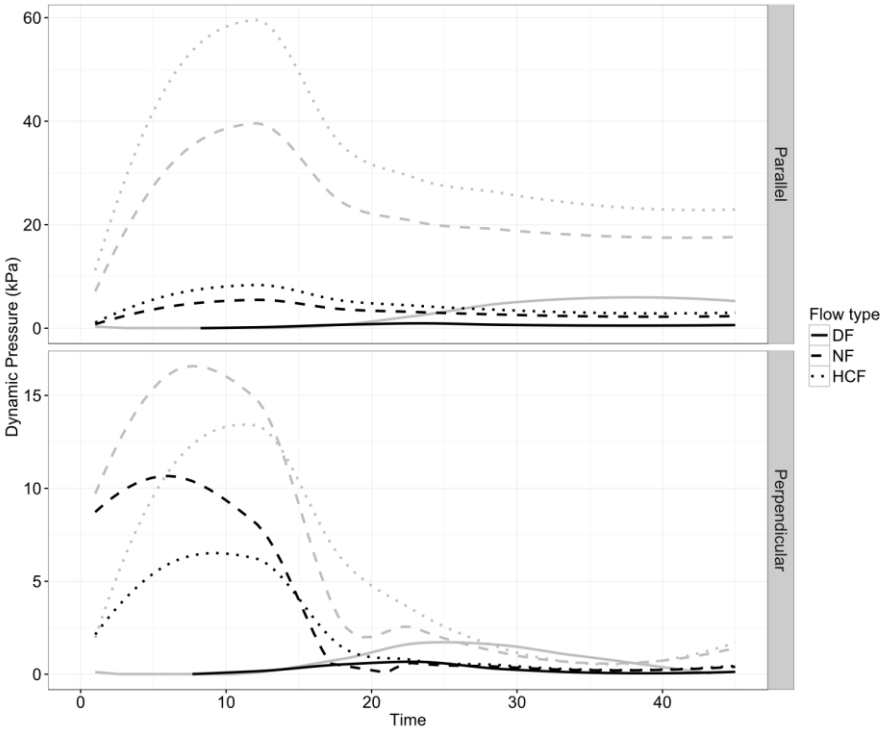

Figure 7. Comparison of mean pressure magnitude (grey lines) and mean normal pressure (black lines) on block 'West 2' in the parallel and perpendicular orientations for a 75 m^3s^{-1} flow along Quebrada Dahlia.

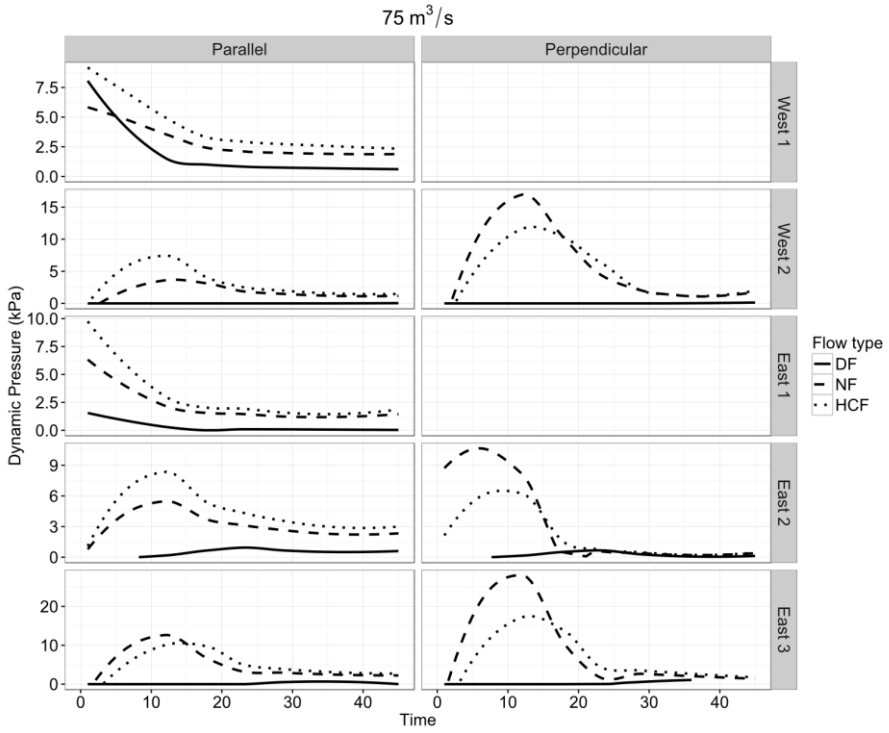

820 **Figure 8. Mean normal pressures applied to each city block in the perpendicular and parallel orientations for a 75 m^3s^{-1} flow.**

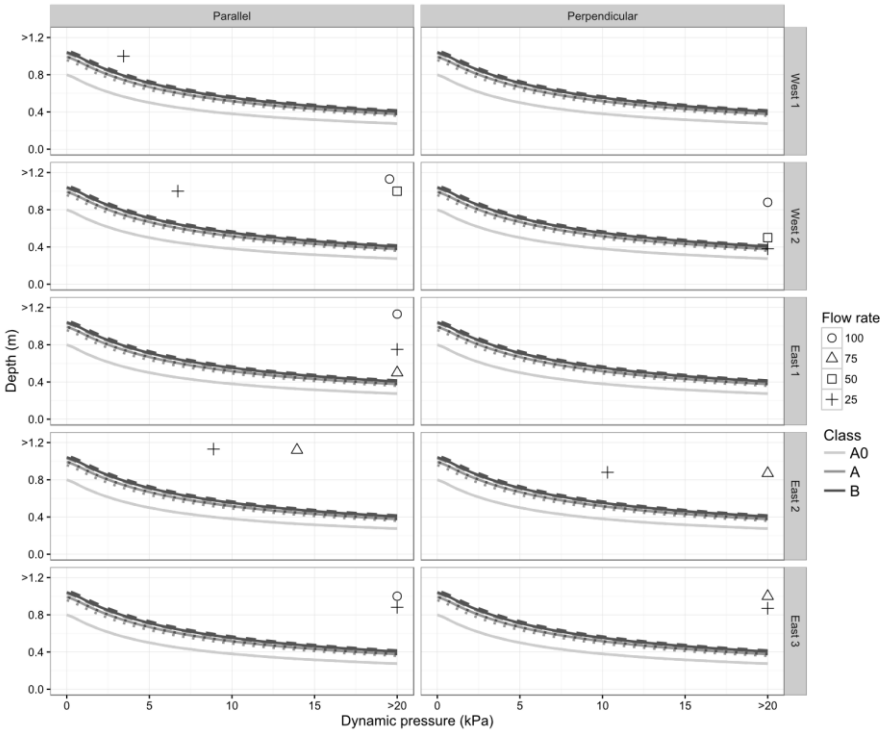
Parallel
Perpendicular
West 1
West 2
East 1
East 2
East 3
Depth (m)
>1.2
0.8
0.4
0.0
0
5
10
15
>20
Dynamic pressure (kPa)
Flow rate
100
75
50
25
Class
A0
A
B

825

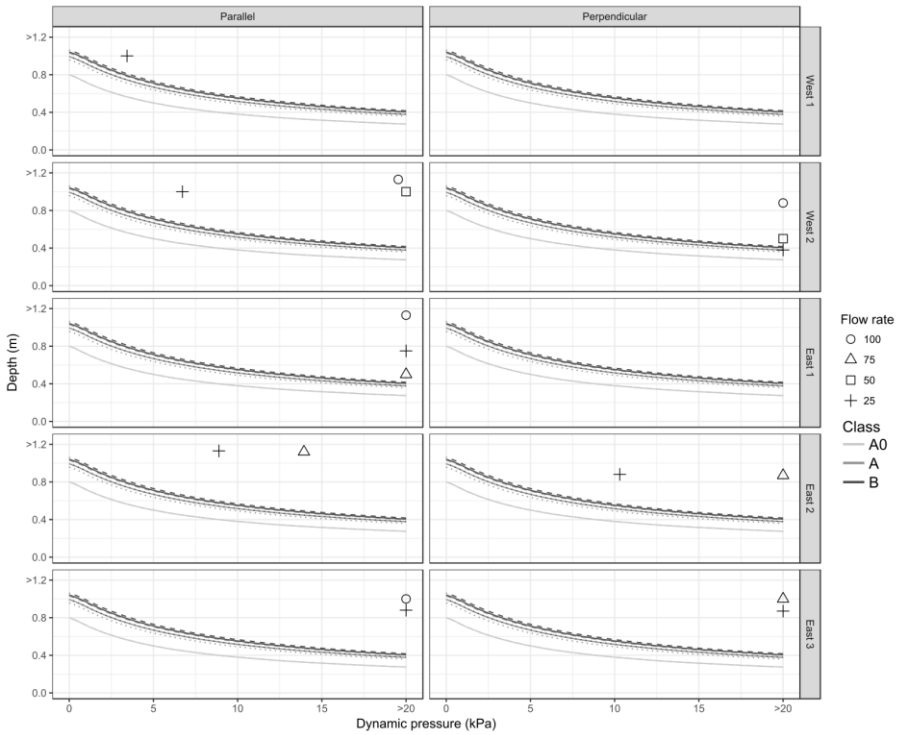

Figure 9. Critical depth-pressure curves for building classes A0, A and B subjected to Newtonian flow. Peak normal pressures and corresponding depths applied to each city block are plotted as points for each flow rate.

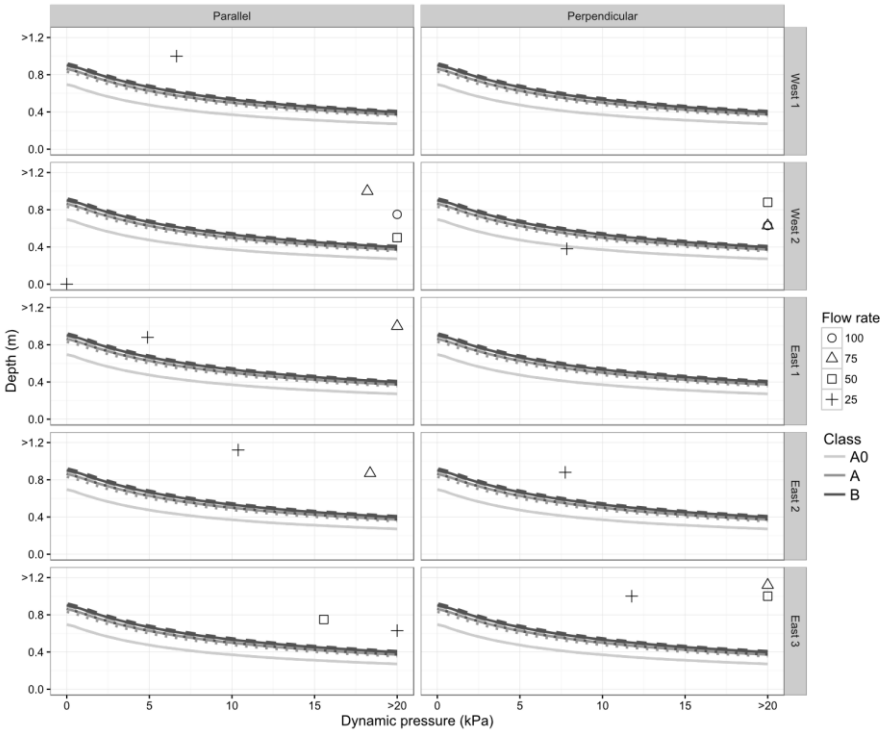
Parallel
Perpendicular
West 1
West 2
East 1
East 2
East 3
Depth (m)
>1.2
0.8
0.4
0.0
0
5
10
15
>20
Dynamic pressure (kPa)
Flow rate
100
75
50
25
Class
A0
A
B

830

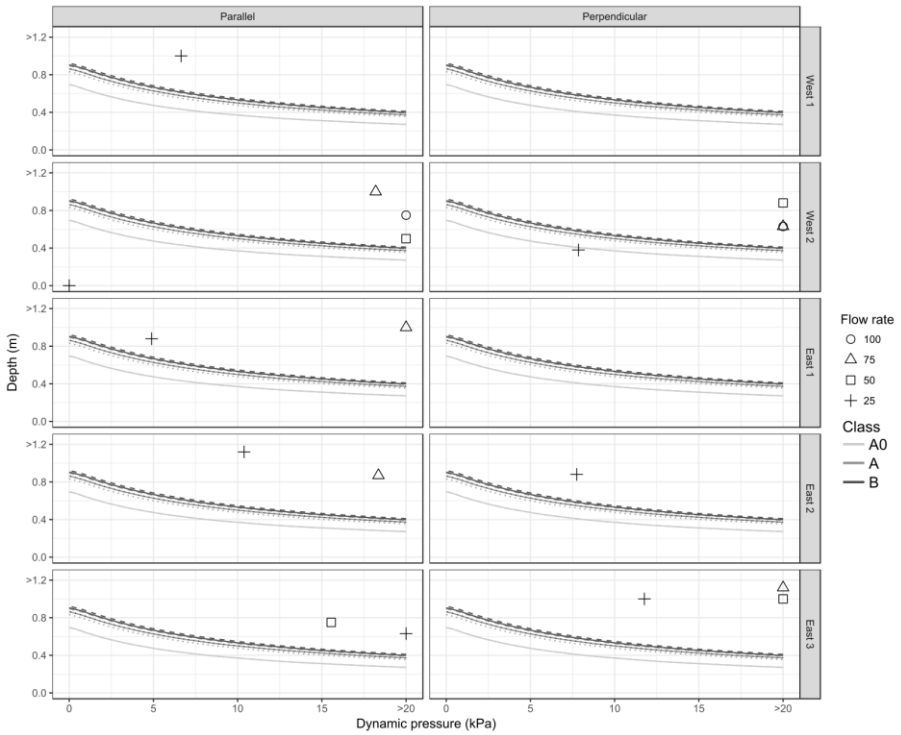

Figure 10. Critical depth-pressure curves for building classes A0, A and B subjected to a hyperconcentrated flow. Peak normal pressures and corresponding depths applied to each city block are plotted as points for each flow rate.

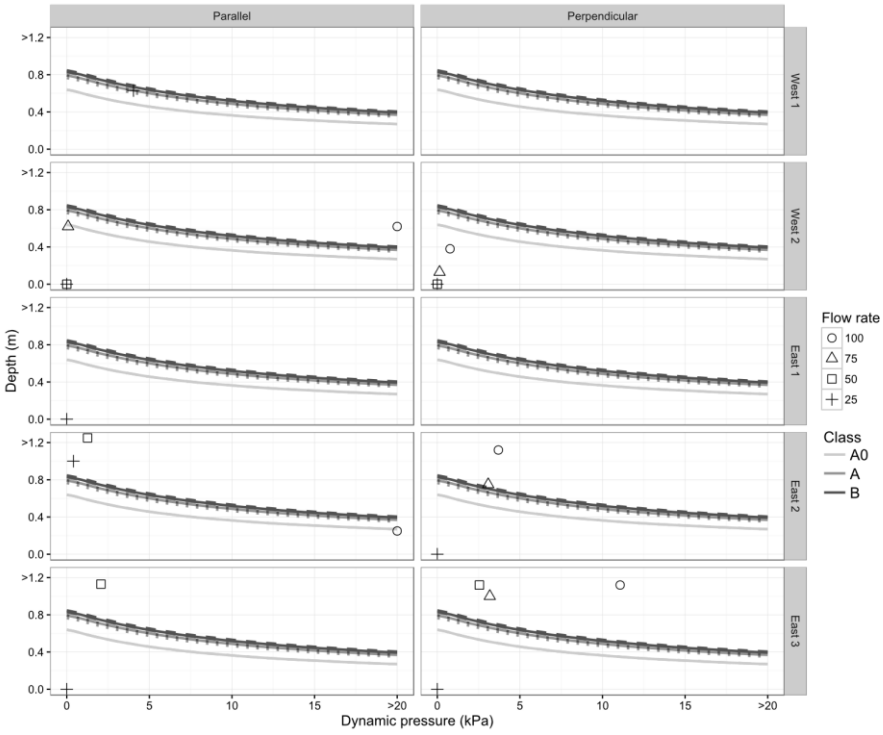
Parallel
Perpendicular
West 1
West 2
East 1
East 2
East 3
Depth (m)
>1.2
0.8
0.4
0.0
0
5
10
15
>20
Dynamic pressure (kPa)
Flow rate
100
75
50
25
Class
A0
A
B

835

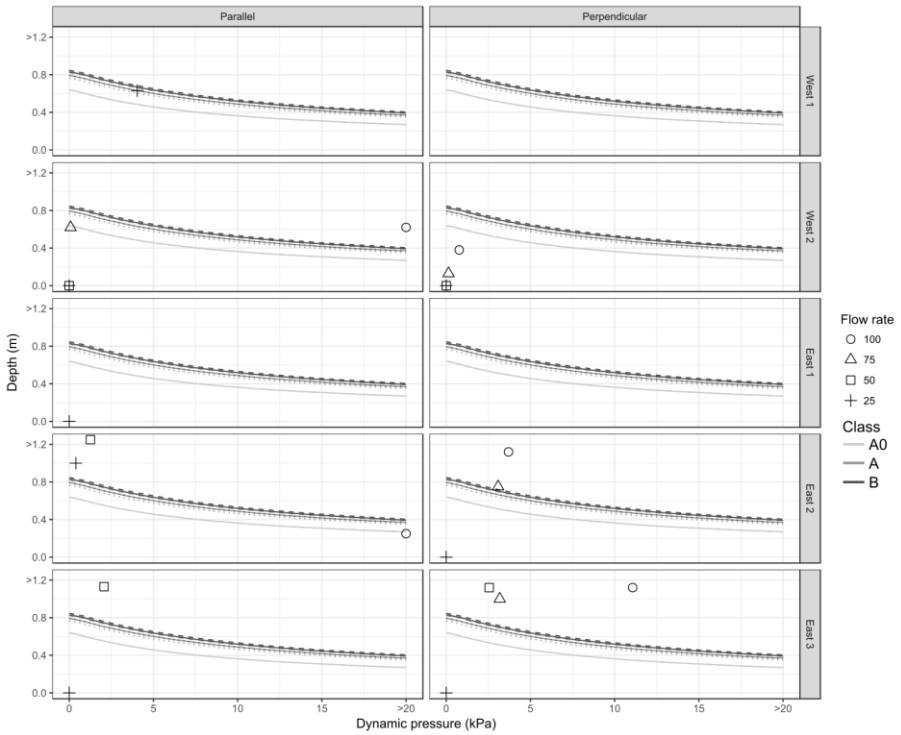

Figure 11. Critical depth-pressure curves for building classes A0, A and B subjected to a debris flow. Peak normal pressures and corresponding depths applied to each city block are plotted as points for each flow rate.

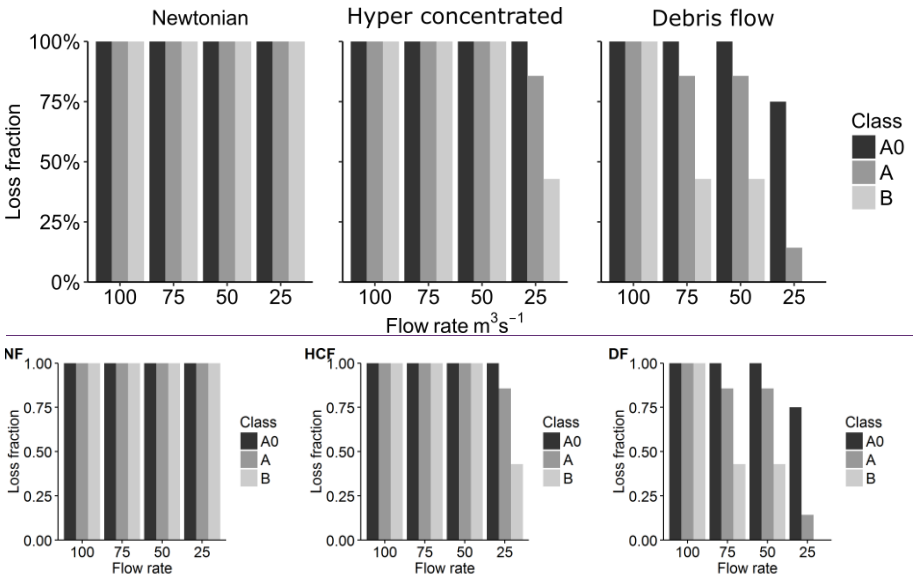

Figure 12. Building loss fraction for all flow scenarios where buildings assumed to have a brick width of 0.15 m.

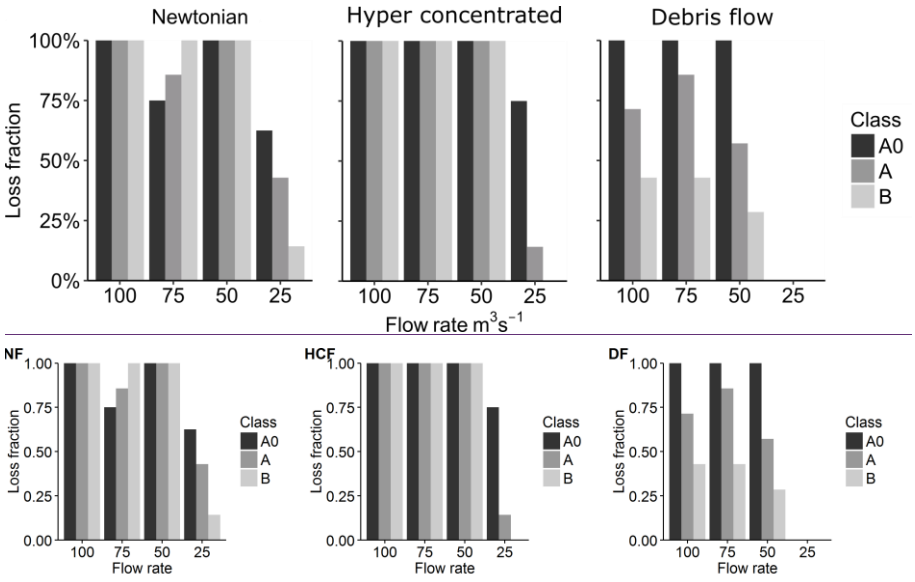

Figure 13. Building loss fraction for all flow scenarios where buildings assumed to have a brick width of 0.25 m.

Tables

Table 1. Individual building type and vulnerability classes for each block in the Quebrada Dahlia study area. Block ID increases from north to south.

Block	ID	Type	Structural class	Structural class	Type	ID	Block
	1	1A	A	A0	2A	1	
	2	1A	A0	A0	2A	2	East 1
	3	4	B	A	3	3	
West 1	4	4	A0	A0	1B	1	
	5	2B	A0	A	3	2	East 2
	6	3	A	A0	1B	3	
	7	4	B	A0	1A	4	
	1	4	B	B	4	1	
	2	4	B	A	3	2	
West 2	3	4	B	A	3	3	East 3
	4	4	B				
	5	3	A				

Table 2. Building types and simplified structural classes from Thouret et al. (2014) ~~(Thouret)~~.

Typology	Building description	Simplified structural class
1A	Unreinforced masonry of lapilli, ignimbrite or terra-cotta with no roof support structure (i.e. metal sheet roof)	A0
1B		A0
2A		A0
2B		A0
3	Terra-cotta masonry with reinforced concrete roof.	A
4	Terra-cotta masonry with reinforced concrete frame and roof.	B
5	Historical ignimbrite building with mortar.	A
6A	Ignimbrite masonry with reinforced concrete elements or modifications.	B
6B		B
6C		B

Table 3. Density, particle concentration and rheology coefficients for hyperconcentrated streamflow and debris flow simulations, taken from Govier et al. (1957); Julien and Lan (1991).

Flow type	Density (kg m^{-3})	Particle concentration by volume (%)	Yield strength (τ_y, Pa)	Viscosity (μ, Pa s)	Dispersive stress coefficient (α)
Hyperconcentrated streamflow	1500	30.3	0.94	0.0137	1.28×10^{-5}
Fine-grained, matrix supported debris flow	1915	55.5	0.672	0.0485	0.00224

Formatted: Not Highlight
Formatted: Caption
Formatted: Highlight
Formatted Table
Formatted: Normal
Formatted: Normal
Formatted: Normal
Formatted: Normal
Formatted: Normal
Formatted: Normal
Formatted: Normal
Formatted: Left
Formatted: Caption